proximately 50% of all patients infected with HCV. A number of individuals with HCV infection are unable to achieve a sustained virological response with the current therapy, and many of them will progress to liver diseases resulting from chronic infection with HCV. Thus, the development of more efficient therapies against HCV is of high priority (Wakita, 2007).

Several in vitro experimental models have been used to investigate the pathology of HCV as well as the efficacy of potential therapeutic compounds. These models include the use of individually cloned proteins of HCV (Littlejohn et al., 1998), infection of primary culture human hepatocytes with HCV (Buck, 2008), and in vitro HCV replicon systems in Huh-7 cells (Bartenschlager, 2005). The HCV replicon systems are particularly useful in HCV research and drug discovery because they are both permissive to high-efficiency HCV replication and respond to antiviral compounds including IFN-$\alpha$ and ribavirin. However, several limitations exist with the use of replicon systems in the discovery and development of novel anti-HCV compounds. These include the cell culture-adaptive mutations of the HCV genome and the innate difference of Huh-7 cells, which are immortalized tumor cells, compared with hepatocytes.

Because of the strict tropism of HCV, only humans and higher primates, such as chimpanzees, have, until recently, been receptive to authentic HCV infection and the development of chronic liver disease due to HCV infection (Lanford et al., 2001; Kremsdorf and Brezillon, 2007). However, use of chimpanzees is difficult from ethical and economical perspectives. The chimeric mouse with a humanized liver on the genetic background of urokinase plasminogen activator-transgenic severe combined immunodeficiency disorder (uPA/SCID) mice, designated as the PXB mouse, has been developed and characterized (Tateno et al., 2004). The livers of these mice are near completely (>70%) replaced with human hepatocytes and maintain the hepatic expression of most human drug-metabolizing enzymes and transporters (Nishimura et al., 2005). Subsequent studies have demonstrated that this mouse model is permissive to the infection of HCV in vivo and has potential utility in the discovery and development of new anti-HCV therapy (Umehara et al., 2006; Hiraga et al., 2007; Inoue et al., 2007). However, one should note that HCV-infected PXB mice do not precisely mimic chronic HCV infection in humans because these mice lack the adaptive immune response and liver disease associated with HCV infection as a result of their genetic background (SCID).

Because the primary organ of HCV infection and its replication is the liver, it is of great importance to know the possible alterations in the hepatic expression and activity of pharmacokinetics-related genes, i.e., drug transporters and metabolizing enzymes, by HCV infection. The aim of the present study was thus to investigate the effect of HCV infection on the mRNA expression of human ABC and SLC transporters and cytochrome P450 enzymes in the livers of PXB mice. Furthermore, the enzymatic activities of major human cytochrome P450 enzymes were compared between noninfected and HCV-infected PXB mice.

## Materials and Methods

**Generation of PXB Mice.** PXB mice were generated by transplanting $1.0 \times 10^6$ human hepatocytes into the spleens of 2- to 3-week-old uPA/SCID mice under diethyl ether anesthesia as described previously (Tateno et al., 2004). All PXB mice used in the present study were derived from the same donor human hepatocyte (BD87, male, 2-year-old white; BD Biosciences, San Jose, CA).

**Inoculation of HCV to PXB Mice.** The inoculum used in the present study was HCV genotype 1b (HCR6, accession no. AY045702), which was obtained from HCV-infected PXB mice at the third passage. The original inoculum was obtained from the serum of an HCV-positive patient. PXB mice with a human albumin concentration in the blood greater than 6.0 mg/ml were infected with HCV genotype 1b at 9 to 10 weeks of age by injecting the inoculum ($1.0 \times 10^4$ copies/mouse) to the retro-orbital sinus under diethyl ether anesthesia.

**Quantification of Human Albumin Concentration and HCV Titer in the Serum.** The concentration of human albumin in mouse blood was determined by latex agglutination immunonephelometry at 13 to 17 weeks of age. The replacement index is defined as the percentage of human hepatocyte repopulated in the host mouse liver and can be estimated from the blood human albumin value. RNA was extracted from the serum of PXB mice using a Sepa Gene RV-R RNA extraction system (Sanko Junyaku Co., Ltd., Ibaraki, Japan) according to the manufacturer's instructions, and the serum titer of HCV was determined by real-time quantitative PCR using TaqMan EZ RT-PCR Core Reagent and an ABI Prism 7500 sequence detector system as described previously (Takeuchi et al., 1999).

**RNA Isolation and TaqMan Gene Expression Assays.** Body weight was measured, and the liver was harvested from each mouse at 17 to 19 weeks of age. Total RNA was isolated from liver specimens using TRIzol (Invitrogen, Carlsbad, CA) according to the manufacturer's instructions and then treated with DNase I to remove contaminating genomic DNA. For cDNA synthesis, 80 ng of RNA was reverse-transcribed using a Transcriptor First Strand cDNA Synthesis Kit (Roche Applied Science, Indianapolis, IN) with random hexamer as the primer. The mRNA expression of human ABC transporters, SLC transporters, cytochrome P450 enzymes, and interferon-stimulated genes (ISGs) was quantified by TaqMan Gene Expression Assays on an ABI Prism 7900 system (Applied Biosystems, Foster City, CA) using LightCycler 480 Probe Master (Roche Applied Science) with primers and FAM-TAMRA or FAM-Iowa Black dual-labeled probes (Integrated DNA Technologies, Inc., Coralville, IA) that are specific for human genes. The protocol for PCR was as follows: 50°C for 2 min, 95°C for 10 min, and 40 cycles of 95°C for 15 s and 60°C for 1 min. The assay identification number or sequences of primers and probes used in the present study are listed in Table 1. The specificities of primers and probes to human genes were confirmed by comparing the amplification from human or mouse liver cDNA. No specific amplification was observed when mouse liver cDNA was used as a PCR template for all genes tested (data not shown). HCV RNA content in the livers of PXB mice was also quantified by TaqMan Gene Expression Assays using a cocktail of three forward primers, one reverse primer, and two TaqMan probes (Table 1) as described previously (Cook et al., 2004). The mRNA expression of each gene was quantified using the comparative $C_t$ method, and normalized by the mRNA expression of hGAPDH.

**Preparation of Liver Microsomes and Determination of Activities of Cytochrome P450 Enzymes.** The microsomal fractions were isolated from the livers of noninfected and HCV-infected PXB mice at 18 or 20 weeks of age as described previously and stored at −70°C until further use (Sugihara et al., 2001). The activities of various P450s were determined in liver microsomes of PXB mice using selective substrates for the human P450 isoforms at appropriate concentrations (Table 2). In brief, 0.2 mg/ml microsomes were preincubated with substrate in 50 mM potassium phosphate buffer (pH 7.4) containing 5 mM $MgCl_2$ at 37°C for 5 min, and, subsequently, 2 mM NADPH was added to start the enzyme reaction. After the incubation at 37°C for 30 min (CYP1A2, CYP2C9, and CYP2C19), 15 min (CYP2D6), or 10 min (CYP3A4), the reaction was terminated by the addition of 150 $\mu$l of acetonitrile containing 7-hydroxycoumarin as an internal standard to 100 $\mu$l of incubation mixture. Samples were then centrifuged at 3000 rpm for 10 min at 4°C to precipitate the protein, and 10 $\mu$l of supernatant was analyzed by liquid chromatography (LC)-tandem mass spectrometry (MS/MS) to quantify the formation of metabolite. For the detection of acetaminophen, the supernatant as well as standard curves were further diluted with 5 mM ammonium acetate to ensure that the signal of each analyte was within the linear range of LC-MS/MS analysis. All of the experiments were conducted in triplicate.

**LC-MS/MS Analysis.** LC-MS/MS was performed on a Shimadzu high-performance liquid chromatography system with two LC-10ADvp pumps and the SCL-10Avp controller (Shimadzu Scientific Instruments, Columbia, MD) and an ABI Sciex API 4000 (Applied Biosystems). Samples were separated on a Hypersil BDS C18 column (50 × 2.1 mm, 5 $\mu$m; Thermo Fisher Scientific, Waltham, MA) with mobile phase A (0.1% formic acid in 5 mM ammonium acetate) and B (0.1% formic acid in acetonitrile/methanol 50/50, v/v) at a flow rate of 0.4 ml/min. High-performance liquid chromatography gradient programs were as follows: for CYP1A2, CYP2C9, and CYP2C19 assays,

TABLE 1

*Assay identification number or sequences of primers and probes used for the TaqMan gene expression assays*

| Gene Name | RefSeq Identification | Assay Identification | Sequences (5′ to 3′) | | |
|---|---|---|---|---|---|
| | | | Forward Primer | Reverse Primer | Probe |
| ABC transporters | | | | | |
| *P-gp* | NM_000927 | Hs01067802_m1 | | | |
| *MDR3* | NM_000443 | | CATCAATGACACCACTGAACTCAA | AACCTTGTCACCAATTCCTTCAC | CGCGGCTAACAGATGACATCTCCAAAA |
| *BSEP* | NM_003742 | | GGGCCATTGTACGAGATCCTAA | TGCACCGTCTTTTCACTTTCTG | TCTTGCTACTAGATGAAGCCACTTCTGCCTTAGA |
| *MRP1* | NM_004996 | | CATCGTGCAGGCGAGTGT | TCCTCACGGTGATGCTGTTC | TGACAGCATCGAGCGACGGCC |
| *MRP2* | NM_000392 | Hs00166123_m1 | | | |
| *MRP3* | NM_003786 | Hs00358656_m1 | | | |
| *MRP4* | NM_005845 | Hs00195260_m1 | | | |
| *BCRP* | NM_004827 | | CAGGTCTGTTGGTCAATCTCACA | TCCATATCGTGGAATGCTGAAG | CCATTGCATCTTGGCTGTCATGGCTT |
| SLC transporters | | | | | |
| *NTCP* | NM_003049 | | CCATGACACCACTCTTGATTGC | CGTCTGCACCGTCCATTG | ACCTCCTCCCTGATGCCTTTTATTGGC |
| *OCT1* | NM_003057 | Hs00427550_m1 | | | |
| *OAT2* | NM_006672 | | CTGCTAGTGTCCTCCGATATGAAG | GCACCGTAGGGTACAACTCTGAA | AAGCTGCCTTCACCACTGCCTACCTG |
| *OATP1B1* | NM_006446 | | GTACCACTTTCTTATTGCAACTCAGACT | CAGGGTGAGATGTAAGTTATTCCATTG | TCCACAGACTGGTTCCCATTGACTTTCA |
| *OATP1B3* | NM_019844 | Hs00251986_m1 | | | |
| *OATP2B1* | NM_007256 | | TCCTGTTTGCAGTGACCATGA | CACCTTCTGGCATCTGGTTAATG | CAGCCTCATGCTGCGCCTTTATGTG |
| Cytochrome P450 enzymes | | | | | |
| *CYP1A1* | NM_000499 | | TGGTCAAGGAGCACTACAAAACC | AGGTCCAAGACGATGTTAATGATCT | ATGAGAACGCCAATGTCCAGCTGTCA |
| *CYP1A2* | NM_000761 | | GGAGACCTTCCGACACTCCTC | CGTTGTGTCCCTTGTTGTGC | TTCTTGCCCTTCACCATCCCCAC |
| *CYP2A6* | NM_000762 | Hs00711162_s1 | | | |
| *CYP2B6* | NM_000767 | | TTGTTCTACCAGACTTTTTCACTCATC | GGAAAGTATTTCAAGAAGCCAGAGA | TCTGTATTCGGCCAGCTGTTTGAGCTC |
| *CYP2C8* | NM_000770 | Hs00426387_m1 | | | |
| *CYP2C9* | NM_000771 | Hs00426397_m1 | | | |
| *CYP2C18* | NM_000772 | Hs00426403_m1 | | | |
| *CYP2C19* | NM_000769 | Hs00426380_m1 | | | |
| *CYP2D6* | NM_000106 | Hs00164385_m1 | | | |
| *CYP2E1* | NM_000773 | Hs00559368_m1 | | | |
| *CYP3A4* | NM_017460 | | CAGGAGGAAATTGATGCAGTTTT | GTCAAGATACTCCATCTGTAGCACAGT | CCCAATAAGGCACCACCCACCTATGA |
| *CYP3A5* | NM_000777 | | TGGACTTTTTAAGAGACTGGGAATTC | AAATTTCCAGAGACCCTGACGAT | CACACCTCTGCCTTTGTTGGGAAATGTT |
| ISGs | | | | | |
| *CIG5* | NM_080657 | | AGATGTTTCTGAAGCGAGGA | GCAGACAATGGCAGTTACTC | TGGATTGGTAGAGCGGAAAGTGGA |
| *G1P2* | NM_005101 | | CTCATCTTTGCCAGTACAGG | AGCTCTGACACCGACAT | CCATGGGCTGGGACCTGACG |
| *G1P3* | NM_002038 | | AAGGCCCTGACCTTCAT | ATTCAGGATCGCAGACCA | AGGAGGACTCGCAGTCGCC |
| *HSXIAPAF1* | NM_017523 | | CTTGAGCACCAGCAGG | GCATGTCCAGTTTGCAGA | TCATAAGGCCAATGAGTGCCAGGA |
| *IFI27* | NM_005532 | | GTAGTTTTGCCCCTGGC | GACATCATCTTGGCTGCT | TGTGATTGGAGGAGTTGTGGCTGT |
| *IFI35* | NM_005533 | | CAAGATGAGGCTGTGGGA | AGACTTAGGCACTTCCGG | CCCCAAAGACAAGGTCCCATTTTCAG |
| *IFI44* | NM_006417 | | GCTACCCTCAGCTCTAGC | CGCTTCCCTCCAAAATGA | ACTGCCATACTTCTTGATCTGTTGTACTGT |
| *IFIT2* | NM_001547 | | AGGAAGATTTCTGAAGAGTGC | GTTCCAGGTGAAATGGCA | CACTGCAACCATGAGTGAGAACAATAAGAA |
| *IFITM1* | NM_003641 | | TCCTCATGACCATTGGATTCATC | CCGTTTTTCCTGTATTATCTGTAACATAA | AGACTGTCACAGAGCCGAATACCA |
| *IRF7* | NM_001572 | | GCAGCGTGAGGGTGTGTCTT | GGAAGCACTCGATGTCGTCAT | CCTGTCCAGCGCCAACAGCC |
| *IRF9/ISGF3G* | NM_006084 | Hs00196051_m1 | | | |
| *MX1* | NM_002462 | | AAGGAATGGGAATCAGTCATGAG | TCTATTAGAGTCAGATCCGGGACAT | CACCCTGGAGATCAGCTCCCGA |
| *MX2* | NM_002463 | | CTAGAGCTTCAGGACCCT | TGATGGTCAGGTCTGGAAC | CGTTCTGGGCTTTGTGTATCTCTTTCTC |
| *OAS1* | NM_016816 | | TGTGTGTCCAAGGTGGTAAAGG | CAACCAGGTCAGCGTCAGATC | CCTCAGGCAAGGGCACCACCCT |
| *OAS2* | NM_016817 | Hs00942643_m1 | | | |
| *OAS3* | NM_006187 | Hs00196324_m1 | | | |
| *OASL* | NM_003733 | Hs00984390_m1 | | | |
| *SP110* | NM_004510 | | CAAAGCGATGAGATCCTGAG | CTGAGTCTTCTTCCGCATTC | CTTGTCATTGGTCACTGAAGTGCTTCT |
| *STAT1* | NM_007315 | | GTGGAAAGACAGCCCTGCAT | ACTGGACCCCTGTCTTCAAGAC | AACGCACCCTCAGAGGCCGC |
| *TLR3* | NM_003265 | Hs01551078_m1 | | | |
| *TNFSF10* | NM_003810 | | TGCGTGCTGATCGTGATCTT | GTACTTGTCCTGCATCTGCTTCA | TGCTCCTGCAGTCTCTCTGTGTGGCT |
| *TRIM22* | NM_006074 | | GCAGGAGTTTGTGACCAA | AGAGGTTCTGTCAGGAGC | CCAAGGGAGCAGTGCAATGGATTT |

DRUG METABOLISM AND DISPOSITION DMD aspet

TABLE 1—*Continued.*

| Gene Name | RefSeq Identification | Assay Identification | Sequences (5′ to 3′) | | |
|---|---|---|---|---|---|
| | | | Forward Primer | Reverse Primer | Probe |
| Others | | | | | |
| *GAPDH* | NM_002046 | | GAAGGTGAAGGTCGGAGTC | GAAGATGGTGATGGGATTTC | CAAGCTTCCCGTTCTCAGCC |
| *HCV* (5′-UTR) | | | GCGACACTCCACCATAGATCACT<br>CGACACTCCACCATGAATCACT<br>CACTCCGCCATGAAYCACT[a] | CACTCGCAAGCACCCTATCA | AGGCCTTTCGCGACCCAACACTACTC<br>AGGCCTTTCGCAACCCAACGCTACT |

UTR, untranslated region.
[a] Y = C or T.

1) mobile phase B was maintained at 5% for 1.0 min, 2) increased linearly to 90% from 1.0 to 2.0 min and maintained to 3.0 min, and 3) brought back to the initial concentration linearly from 3.0 to 3.1 min for reequilibration, total run time 4.0 min; for CYP2D6 assay, 1) mobile phase B was maintained at 5% for 1.0 min, 2) increased linearly to 95% from 1.0 to 2.0 min and maintained to 4.0 min, and 3) brought back to the initial concentration linearly from 4.0 to 4.1 min for reequilibration, total run time 6.0 min; and for CYP3A4 assay, 1) mobile phase B was maintained at 5% for 1.0 min, 2) increased linearly to 95% from 1.0 to 2.0 min and maintained to 3.0 min, and 3) brought back to the initial concentration linearly from 3.0 to 3.1 min for reequilibration, total run time 4.0 min. The MS/MS parameters and linear range of standard curves (limit of detection to maximum concentration) are listed for each metabolite in Table 2. Data were collected and processed using Sciex Analyst 1.4.2 data collection and integration software.

**Statistical Analysis.** Statistical analysis was performed by Student's *t* test using GraphPad Prism (version 4). Asterisks represent significant differences (*, $P < 0.05$, **, $P < 0.01$, and ***, $P < 0.001$, respectively) between noninfected and HCV-infected PXB mice.

## Results

**Human Albumin Concentration and HCV Titers in PXB Mice.** Sex, human albumin concentration in the blood, body weight, serum HCV titers, and HCV RNA content in the liver are summarized in Table 3 for each mouse. The sex of PXB mice did not affect the activity of human cytochrome P450 enzymes derived from the human hepatocytes inside the host mouse liver (supplemental data). The average concentration of human albumin in the blood was not significantly different between noninfected and HCV-infected PXB mice. Accordingly, the replacement index of human hepatocytes estimated from the albumin concentration was similar between the two groups. Although body weight at the time of liver isolation was significantly higher in HCV-infected PXB mice than in noninfected mice for those used for the preparation of total liver RNA, the difference was not statistically significant in those used for the preparation of liver microsomes. Indeed, unpublished observations (C. Tateno) with different batches of HCV-infected mice suggested that HCV infection does not significantly affect the body weight of either male or female PXB mice. Serum HCV titers were determined in HCV-infected PXB mice, and HCV RNA content in the liver was measured in both noninfected and HCV-infected groups. A significant amount of HCV RNA was detected in both the serum and liver of HCV-infected mice, whereas HCV RNA was not detected in the liver of noninfected mice. These results confirmed that PXB mice were successfully infected by HCV.

**Activation of Interferon-Signaling Pathways in HCV-Infected PXB Mice.** Previous reports suggested that chronic infection with HCV is accompanied by the up-regulation of genes related to the interferon-signaling pathways in human patients (Smith et al., 2006). To corroborate the relevance of our experimental model in PXB mice to clinical HCV infection, the mRNA expression of human ISGs observed to be activated in HCV-infected patients was quantified in the livers of noninfected and HCV-infected mice. Fourteen of 22 ISGs investigated exhibited a significant increase in mRNA expression in the livers of HCV-infected PXB mice compared with that in noninfected mice (Fig. 1). The mRNA expression of MX2 was below the limit of detection in both groups. These results suggest that the interferon signaling pathways are activated by HCV infection in PXB mice, which is similar to what is observed in patients with chronic HCV infection.

**mRNA Expression of Human ABC and SLC Transporters.** The mRNA expression of major human hepatic ABC and SLC transporters was quantified in the livers of noninfected and HCV-infected PXB mice (Fig. 2). A significant increase in mRNA expression was ob-

TABLE 2

*Substrate concentration and analytical parameters for each metabolite in MS/MS*

| Enzyme | Substrate | Metabolite | Mass Transition (*m/z*) | Mode | CE | DP | Linear Range |
|---|---|---|---|---|---|---|---|
| | | | | | *eV* | *eV* | |
| CYP1A2 | Phenacetin (10 μM) | Acetaminophen | 152.13 > 110.15 | ESI+ | 22 | 46 | 10 nM–10 μM |
| CYP2C9 | Diclofenac (5 μM) | 4′-Hydroxydiclofenac | 312.09 > 230.01 | ESI+ | 45 | 41 | 1 nM–1 μM |
| CYP2C19 | (*S*)-Mephenytoin (50 μM) | 4′-Hydroxymephenytoin | 235.10 > 150.21 | ESI+ | 24 | 56 | 1 nM–1 μM |
| CYP2D6 | Dextromethorphan (5 μM) | Dextrorphan | 258.17 > 157.10 | ESI+ | 51 | 81 | 1 nM–1 μM |
| CYP3A4 | Midazolam (1 μM) | 1′-Hydroxymidazolam | 341.82 > 203.20 | ESI+ | 38 | 71 | 1 nM–1 μM |

CE, collision energy; DP, declustering potential; ESI, electrospray ionization.

TABLE 3

*Human albumin concentration, estimated replacement index, body weight, and HCV content in the serum and liver of PXB mice*

| Animal | Sex | h-Alb | Estimated RI | Body Weight | Serum HCV Titer ($10^7$ copies/ml) | HCV RNA Content in the Liver (Relative to hGAPDH) |
|---|---|---|---|---|---|---|
| | | *mg/ml* | % | *g* | | |
| PXB mice used for the preparation of total liver RNA | | | | | | |
| Noninfected | | | | | | |
| PXB41-18 | Male | 6.3 | 74.2 | 14.4 | —[a] | N.D. |
| PXB41-25 | Male | 8.2 | 82.3 | 13.7 | — | N.D. |
| PXB42-I | Male | 12.2 | 94.6 | 15.0 | — | N.D. |
| Mean ± S.D. | | 8.9 ± 3.0 | 83.7 ± 10.3 | 14.3 ± 0.6 | — | — |
| HCV-infected | | | | | | |
| PXB36-11 | Male | 5.3 | 68.9 | 17.2 | 5.15 | $4.95 \times 10^{-3}$ |
| PXB36-23 | Male | 7.7 | 80.4 | 16.8 | 5.52 | $3.53 \times 10^{-3}$ |
| PXB38-11 | Male | 5.8 | 71.7 | 16.2 | 2.12 | $3.16 \times 10^{-3}$ |
| Mean ± S.D. | | 6.3 ± 1.3 | 73.7 ± 6.0 | 16.7 ± 0.5* | 4.26 ± 1.87 | $3.88 \times 10^{-3} \pm 9.46 \times 10^{-4}$ |
| PXB mice used for the preparation of liver microsomes | | | | | | |
| Noninfected | | | | | | |
| PXB22-47 | Female | 6.3 | 74.2 | 19.8 | — | — |
| PXB22-48 | Female | 7.3 | 78.7 | 11.5 | — | — |
| PXB22-57 | Female | 5.2 | 68.2 | 14.7 | — | — |
| Mean ± S.D. | | 6.3 ± 1.1 | 73.7 ± 5.3 | 15.3 ± 4.2 | — | — |
| HCV-infected | | | | | | |
| PXB86-13 | Male | 6.3 | 74.2 | 22.8 | 6.56 | — |
| PXB86-26 | Female | 3.5 | 55.9 | 19.4 | 0.806 | — |
| PXB86-33 | Male | 6.4 | 74.6 | 22.1 | 4.66 | — |
| Mean ± S.D. | | 5.4 ± 1.6 | 68.2 ± 10.7 | 21.4 ± 1.8 | 4.01 ± 2.93 | — |

h-Alb, human albumin; RI, replacement index; N.D., not detected.
* $P < 0.01$, significantly different between noninfected and HCV-infected PXB mice.
[a] —, not determined.

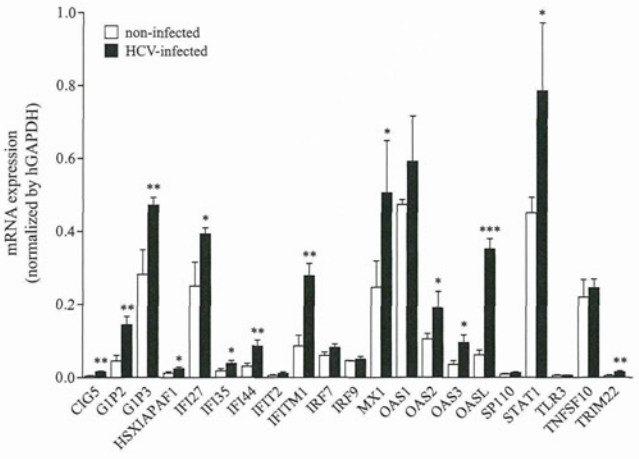


FIG. 1. Activation of interferon signaling pathways in HCV-infected PXB mice. The mRNA expression of human interferon-stimulated genes was measured in the livers of noninfected and HCV-infected PXB mice by TaqMan Gene Expression Assays as described under *Materials and Methods*, and the data were normalized by the mRNA expression of hGAPDH. Results are presented as the mean ± S.D. of three mice. □, mRNA expression in noninfected PXB mice; ■, mRNA expression in HCV-infected PXB mice. *, $P < 0.05$; **, $P < 0.01$; ***, $P < 0.001$, significantly different between noninfected and HCV-infected mice.

served for MRP4 and OATP2B1 in HCV-infected PXB mice compared with that in noninfected mice. In contrast, OCT1 was significantly decreased in HCV-infected PXB mice compared with that in their noninfected controls. The mRNA expression of MRP1 was below the limit of detection in both noninfected and HCV-infected groups. The mRNA levels of other ABC and SLC transporters, including P-gp, MDR3, BSEP, MRP2, MRP3, NTCP, OAT2, OATP1B1, and OATP1B3, were comparable between the two groups.

**mRNA Expression of Human Cytochrome P450 Enzymes.** The mRNA expression of 12 human cytochrome P450 genes, *CYP1A1*, *CYP1A2*, *CYP2A6*, *CYP2B6*, *CYP2C8*, *CYP2C9*, *CYP2C18*, *CYP2C19*, *CYP2D6*, *CYP2E1*, *CYP3A4*, and *CYP3A5*, was investigated in the livers of noninfected and HCV-infected PXB mice (Fig. 3). The mRNA expression of these genes was not statistically different between the two groups with the exception of significantly lower expression of CYP2D6 in HCV-infected mice.

**Activity of Human Cytochrome P450 Enzymes.** The activities of five major human cytochrome P450 enzymes, namely, CYP1A2, CYP2C9, CYP2C19, CYP2D6, and CYP3A4, were investigated in the liver microsomes of noninfected and HCV-infected PXB mice (Fig. 4). The metabolic activity in the liver microsomes from uPA/SCID mice for each probe substrate was comparable to or lower than that in human liver microsomes (C. Tateno, unpublished observations). Taking into account the fact that the livers of PXB mice are nearly completely (>70%) replaced with human hepatocytes, the background activity from remaining mouse hepatocyte in PXB

DMD DRUG METABOLISM AND DISPOSITION aspet

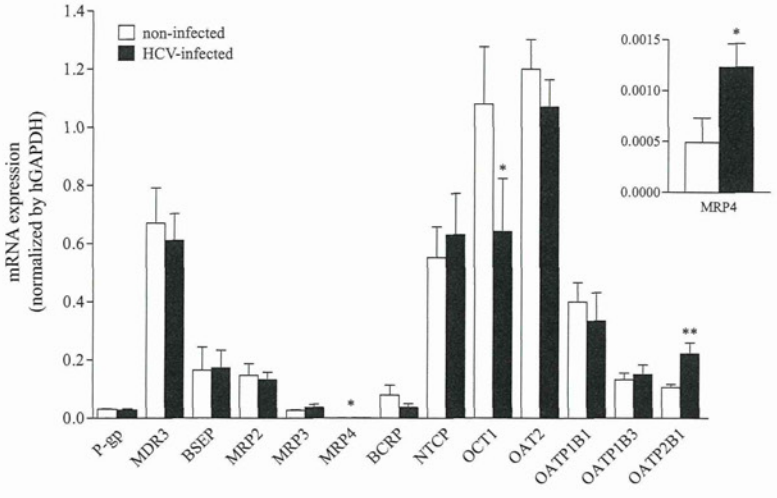


FIG. 2. mRNA expression profiles of drug transporters in PXB mice. The mRNA expression of human ABC and SLC transporters was measured in the livers of noninfected (□) and HCV-infected (■) PXB mice by TaqMan Gene Expression Assays, and the data are presented as described in the legend to Fig. 1. The inset represents the magnification of the mRNA expression of MRP4.

mice is minor. The metabolic activity of CYP1A2 was significantly lower in HCV-infected PXB mice than in noninfected PXB mice. The activities of other P450s were similar between noninfected and HCV-infected PXB mice.

## Discussion

In the present study, the effect of HCV infection on the mRNA expression profiles of human ABC and SLC transporters and cytochrome P450 enzymes in PXB mice was investigated. The primers and probes specific for human genes were used in the TaqMan gene expression assays to exclude the background amplification of homologous genes from the host mouse liver. In addition, we have characterized enzymatic activities of major human P450s in the microsomes isolated from the livers of PXB mice.

The body weight and human albumin concentration in the blood of PXB mice were similar between noninfected and HCV-infected groups, suggesting that the inoculation of HCV does not affect the growth of transplanted human hepatocytes inside the host mouse liver or maturation of the mice (Table 3). A profound effect of HCV infection was observed on the status of interferon-signaling pathways, for which mRNA expression of a series of ISGs was significantly higher in the livers of HCV-infected PXB mice compared with that of noninfected controls (Fig. 1). The up-regulation of ISGs are in good agreement with the observation in patients with chronic HCV infection and chimpanzees with acute HCV infection (Su et al., 2002; Smith et al., 2006). In addition, these data are similar to the results published previously by Walters et al. (2006) who also used the human hepatocyte chimeric mouse model to examine the regulation of overall hepatic gene expression by HCV genotype 1a infection with microarray technology. It is of note that the effect of HCV infection on the expression of ISGs was comparable between genotype 1a (Walters et al., 2006) and 1b (this study). It is likely that there is no marked difference between the two HCV genotypes in terms of their effects on gene expression. It has been previously demonstrated that viremia in PXB mice can be reduced by treatment with IFN-$\alpha$ or pegylated-IFN as in human patients (Umehara et al., 2006; Hiraga et al., 2007; Inoue et al., 2007). The presence of functional interferon signaling pathways in PXB mice, suggested by the up-regulation of a number of ISGs by HCV infection, provides a rationale for the efficacy of those antiviral agents in this model. These observations warrant the use of PXB mice as an in vivo model for the primary infection of the liver by HCV to investigate the effects of novel anti-HCV compounds on suppressing the replication of HCV.

There were, in general, few marked differences in the mRNA expression of human ABC and SLC transporters and cytochrome P450 enzymes in the liver between noninfected and HCV-infected PXB mice with some exceptions, e.g., significantly higher expression

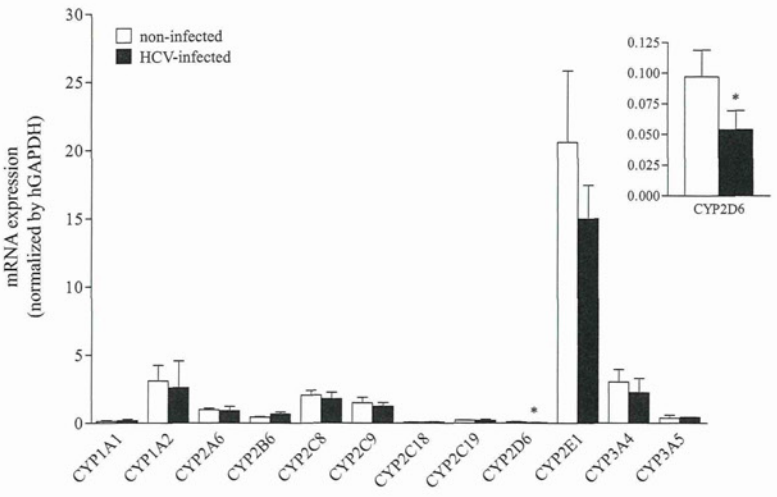


FIG. 3. mRNA expression profiles of drug-metabolizing enzymes in PXB mice. The mRNA expression of human cytochrome P450 enzymes was measured in the livers of noninfected (□) and HCV-infected (■) PXB mice by TaqMan Gene Expression Assays, and the data are presented as described in the legend to Fig. 1. The inset represents the magnification of the mRNA expression of CYP2D6.

DRUG METABOLISM AND DISPOSITION DMD aspet

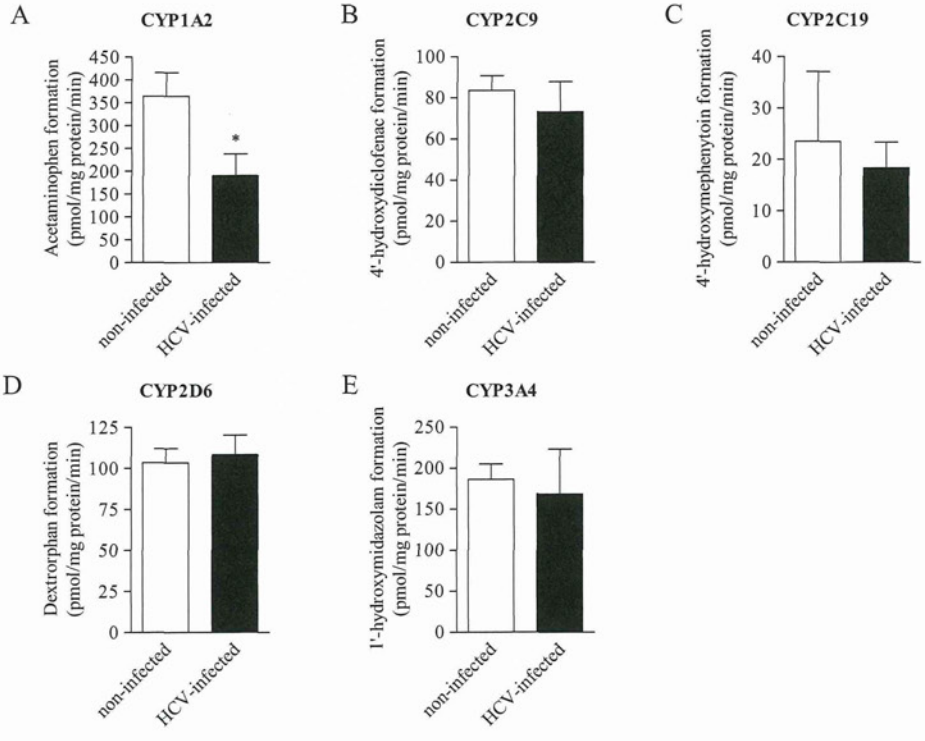


FIG. 4. Activity of human cytochrome P450 enzymes in PXB mice. The activities of five major human cytochrome P450 enzymes, i.e., CYP1A2 (A), CYP2C9 (B), CYP2C19 (C), CYP2D6 (D), and CYP3A4 (E), were measured in the liver microsomes of noninfected and HCV-infected PXB mice as described under *Materials and Methods*. Results are presented as the mean ± S.D. of three mice. □, metabolic activity in noninfected PXB mice; ■, metabolic activity in HCV-infected PXB mice. *, $P < 0.05$, significantly different between noninfected and HCV-infected mice.

of MRP4 and OATP2B1 and lower expression of OCT1 and CYP2D6 in HCV-infected mice than in noninfected mice (Figs. 2 and 3). Likewise, the activities of major human cytochrome P450 enzymes were similar between noninfected and HCV-infected PXB mice except for CYP1A2, which exhibited a significantly lower activity in HCV-infected PXB mice than in noninfected mice (Fig. 4). The effect of HCV infection on the mRNA expression and enzymatic activity of CYP1A2 and CYP2D6 was not consistent. The change in mRNA expression of CYP2D6 might not be sufficient to affect its enzymatic activity, whereas posttranscriptional effects of HCV infection may explain the decreased enzymatic activity of CYP1A2 regardless of unchanged mRNA expression. In consideration of the induction of many ISGs at the mRNA level, it is likely that the effect of HCV infection on the expression of pharmacokinetics-related genes would also be observed, if any, at the transcriptional level (CYP1A2 might be an exception). HCV infection probably affects gene expression via direct interference by virus infection, that is, the innate antiviral response and/or indirect interference by adaptive HCV-specific immune response, oxidative stress, and liver disease associated with chronic infection (Pawlotsky, 1998; Missale et al., 2004). PXB mice are immunocompromised because of their genetic background and thus lack the adaptive immune response and liver disease associated with HCV infection: i.e., there was no hepatocyte damage or inflammation in the liver of infected chimeric mice (Hiraga et al., 2007). HCV infection will thus affect gene expression only through the innate antiviral response in our experimental model. The similar expression profiles of drug transporters and metabolizing enzymes between noninfected and HCV-infected PXB mice suggest that innate antiviral signaling pathways play only a minor role in the regulation of mRNA expression of these genes.

There have been several reports regarding the aberrant mRNA expression of drug transporters and metabolizing enzymes in patients with HCV infection compared with those without infection or healthy volunteers. Hinoshita et al. (2001) have demonstrated that the mRNA expression of P-gp, MDR3, MRP1, MRP2, and MRP3 in the noncancerous region in the liver of patients with hepatic tumor tends to be lower in HCV-infected groups than in noninfected ones. On the other hand, Ros et al. (2003) have reported increased mRNA expression of P-gp and MRP3 in the livers of patients with HCV infection compared with healthy volunteers, whereas there was no significant difference for MRP2. Nakai et al. (2001) have performed a comprehensive study of variation in the mRNA levels of drug transporters and metabolizing enzymes in patients with chronic hepatitis C using quantitative real-time PCR and observed clear correlations between fibrosis stage and mRNA levels of CYP1A2, CYP2E1, CYP3A4, NTCP, OCT1, and OATP1B1 in the liver, whereas no fibrosis stage-dependent differences were observed for other transporters and enzymes that included P-gp, MDR3, MRP1, MRP2, and MRP3 (Nakai et al., 2008). Intriguingly, these clinical observations are inconsistent with the present findings in PXB mice in which HCV infection affects gene expression primarily through the innate antiviral response. The altered expression of drug transporters and metabolizing enzymes in clinical patients might be ascribed to the indirect interference by HCV infection or secondary effects as a result of the development of liver fibrosis or other hepatic dysfunction resulting from HCV infection. Indeed, serum levels or spontaneous productions by peripheral blood mononuclear cells of inflammatory cytokines such as tumor necrosis factor-$\alpha$, interleukin-1$\beta$, and interleukin-6 were elevated in HCV-infected patients compared with those in healthy subjects (Kishihara et al., 1996; Huang et al., 1999; Cotler et al., 2001). In addition, several lines of evidence suggest perturbation of the expression of drug transporters and metabolizing enzymes by these cytokines both in vivo and in vitro (Lee and Piquette-Miller, 2003; Geier et al., 2005; Renton, 2005; Vee et al., 2009). Oxidative stress and liver diseases including cirrhosis and hepatocellular carcinoma, which are prevalent in patients with chronic HCV infection, also compromise the physiological expression of drug transporters (Bonin et al., 2002; Toyoda et al., 2008). This complex nature of HCV infection and progression to liver disease may

account for the controversial findings regarding the expression of pharmacokinetics-related genes in clinical patients with HCV infection, although the possibility of a difference in the patient population cannot be ruled out.

Because all PXB mice used in the present study are derived from a single donor hepatocyte, future studies are necessary to generalize the present findings by characterizing different batches of PXB mice originated from other donor hepatocytes. Nevertheless, the present study has clearly demonstrated that the infection of PXB mice, the chimeric mice with humanized liver, by HCV triggers the activation of interferon-signaling pathways as observed in human patients with chronic infection, but in general does not have a significant impact on the mRNA expression profiles of human ABC and SLC transporters or on the mRNA expression and enzymatic activity of cytochrome P450 enzymes. These results suggest that the pharmacokinetic behavior of small molecule antiviral therapies such as protease and polymerase inhibitors is likely to be comparable between HCV-infected and noninfected PXB mice. The PXB mouse model is a good model to study the effects of novel anti-HCV compounds in the primary treatment of HCV infection on suppressing the replication of HCV and therefore to investigate the relationship of the pharmacokinetics and pharmacodynamics of such therapies. However, caution is needed in the translation of this relationship to HCV-infected patients because PXB mice are immunocompromised based on their genetic background (SCID), and thus this mouse model does not accurately reflect the liver disease and immune response such as the increase in the levels of inflammatory cytokines observed in patients with chronic HCV infection, which may lead to changes in drug transporter and metabolizing enzyme expression.

**Acknowledgments.** We thank Drs. Yasuhisa Adachi and Shin-ichi Ninomiya for their technical assistance in the microsome assays.

## References


Bartenschlager R (2005) The hepatitis C virus replicon system: from basic research to clinical application. *J Hepatol* **43:**210–216.

Bonin S, Pascolo L, Crocé LS, Stanta G, and Tiribelli C (2002) Gene expression of ABC proteins in hepatocellular carcinoma, perineoplastic tissue, and liver diseases. *Mol Med* **8:**318–325.

Buck M (2008) Direct infection and replication of naturally occurring hepatitis C virus genotypes 1, 2, 3 and 4 in normal human hepatocyte cultures. *PLoS One* **3:**e2660.

Chandra P and Brouwer KL (2004) The complexities of hepatic drug transport: current knowledge and emerging concepts. *Pharm Res* **21:**719–735.

Cook L, Ng KW, Bagabag A, Corey L, and Jerome KR (2004) Use of the MagNA pure LC automated nucleic acid extraction system followed by real-time reverse transcription-PCR for ultrasensitive quantitation of hepatitis C virus RNA. *J Clin Microbiol* **42:**4130–4136.

Cotler SJ, Reddy KR, McCone J, Wolfe DL, Liu A, Craft TR, Ferris MW, Conrad AJ, Albrecht J, Morrissey M, Ganger DR, Rosenblate H, Blatt LM, Jensen DM, and Taylor MW (2001) An analysis of acute changes in interleukin-6 levels after treatment of hepatitis C with consensus interferon. *J Interferon Cytokine Res* **21:**1011–1019.

Dobson PD and Kell DB (2008) Carrier-mediated cellular uptake of pharmaceutical drugs: an exception or the rule? *Nat Rev Drug Discov* **7:**205–220.

Geier A, Dietrich CG, Voigt S, Ananthanarayanan M, Lammert F, Schmitz A, Trauner M, Wasmuth HE, Boraschi D, Balasubramaniyan N, Suchy FJ, Matern S, and Gartung C (2005) Cytokine-dependent regulation of hepatic organic anion transporter gene transactivators in mouse liver. *Am J Physiol Gastrointest Liver Physiol* **289:**G831–G841.

Gonzalez FJ (1990) Molecular genetics of the P-450 superfamily. *Pharmacol Ther* **45:**1–38.

Hinoshita E, Taguchi K, Inokuchi A, Uchiumi T, Kinukawa N, Shimada M, Tsuneyoshi M, Sugimachi K, and Kuwano M (2001) Decreased expression of an ATP-binding cassette transporter, MRP2, in human livers with hepatitis C virus infection. *J Hepatol* **35:**765–773.

Hiraga N, Imamura M, Tsuge M, Noguchi C, Takahashi S, Iwao E, Fujimoto Y, Abe H, Maekawa T, Ochi H, Tateno C, Yoshizato K, Sakai A, Sakai Y, Honda M, Kaneko S, Wakita T, and Chayama K (2007) Infection of human hepatocyte chimeric mouse with genetically engineered hepatitis C virus and its susceptibility to interferon. *FEBS Lett* **581:**1983–1987.

Huang YS, Hwang SJ, Chan CY, Wu JC, Chao Y, Chang FY, and Lee SD (1999) Serum levels of cytokines in hepatitis C-related liver disease: a longitudinal study. *Zhonghua Yi Xue Za Zhi (Taipei)* **62:**327–333.

Inoue K, Umehara T, Ruegg UT, Yasui F, Watanabe T, Yasuda H, Dumont JM, Scalfaro P, Yoshiba M, and Kohara M (2007) Evaluation of a cyclophilin inhibitor in hepatitis C virus-infected chimeric mice in vivo. *Hepatology* **45:**921–928.

Kishihara Y, Hayashi J, Yoshimura E, Yamaji K, Nakashima K, and Kashiwagi S (1996) IL-1$\beta$ and TNF-$\alpha$ produced by peripheral blood mononuclear cells before and during interferon therapy in patients with chronic hepatitis C. *Dig Dis Sci* **41:**315–321.

Kremsdorf D and Brezillon N (2007) New animal models for hepatitis C viral infection and pathogenesis studies. *World J Gastroenterol* **13:**2427–2435.

Lanford RE, Bigger C, Bassett S, and Klimpel G (2001) The chimpanzee model of hepatitis C virus infections. *ILAR J* **42:**117–126.

Lee G and Piquette-Miller M (2003) Cytokines alter the expression and activity of the multidrug resistance transporters in human hepatoma cell lines; analysis using RT-PCR and cDNA microarrays. *J Pharm Sci* **92:**2152–2163.

Littlejohn M, Locarnini S, and Bartholomeusz A (1998) Targets for inhibition of hepatitis C virus replication. *Antivir Ther* **3:**83–91.

Meyer UA (1996) Overview of enzymes of drug metabolism. *J Pharmacokinet Biopharm* **24:**449–459.

Missale G, Cariani E, and Ferrari C (2004) Role of viral and host factors in HCV persistence: which lesson for therapeutic and preventive strategies? *Dig Liver Dis* **36:**703–711.

Nakai K, Tanaka H, Hanada K, Ogata H, Suzuki F, Kumada H, Miyajima A, Ishida S, Sunouchi M, Habano W, Kamikawa Y, Kubota K, Kita J, Ozawa S, and Ohno Y (2008) Decreased expression of cytochromes P450 1A2, 2E1, and 3A4 and drug transporters $Na^+$-taurocholate-cotransporting polypeptide, organic cation transporter 1, and organic anion-transporting peptide-C correlates with the progression of liver fibrosis in chronic hepatitis C patients. *Drug Metab Dispos* **36:**1786–1793.

Nishimura M, Yoshitsugu H, Yokoi T, Tateno C, Kataoka M, Horie T, Yoshizato K, and Naito S (2005) Evaluation of mRNA expression of human drug-metabolizing enzymes and transporters in chimeric mouse with humanized liver. *Xenobiotica* **35:**877–890.

Pawlotsky JM (1998) Hepatitis C virus infection: virus/host interactions. *J Viral Hepat* **5(Suppl 1):**3–8.

Rendic S and Di Carlo FJ (1997) Human cytochrome P450 enzymes: a status report summarizing their reactions, substrates, inducers, and inhibitors. *Drug Metab Rev* **29:**413–580.

Renton KW (2005) Regulation of drug metabolism and disposition during inflammation and infection. *Expert Opin Drug Metab Toxicol* **1:**629–640.

Ros JE, Libbrecht L, Geuken M, Jansen PL, and Roskams TA (2003) High expression of MDR1, MRP1, and MRP3 in the hepatic progenitor cell compartment and hepatocytes in severe human liver disease. *J Pathol* **200:**553–560.

Shitara Y, Horie T, and Sugiyama Y (2006) Transporters as a determinant of drug clearance and tissue distribution. *Eur J Pharm Sci* **27:**425–446.

Smith MW, Walters KA, Korth MJ, Fitzgibbon M, Proll S, Thompson JC, Yeh MM, Shuhart MC, Furlong JC, Cox PP, Thomas DL, Phillips JD, Kushner JP, Fausto N, Carithers RL Jr, and Katze MG (2006) Gene expression patterns that correlate with hepatitis C and early progression to fibrosis in liver transplant recipients. *Gastroenterology* **130:**179–187.

Su AI, Pezacki JP, Wodicka L, Brideau AD, Supekova L, Thimme R, Wieland S, Bukh J, Purcell RH, Schultz PG, and Chisari FV (2002) Genomic analysis of the host response to hepatitis C virus infection. *Proc Natl Acad Sci USA* **99:**15669–15674.

Sugihara K, Kitamura S, Yamada T, Ohta S, Yamashita K, Yasuda M, and Fujii-Kuriyama Y (2001) Aryl hydrocarbon receptor (AhR)-mediated induction of xanthine oxidase/xanthine dehydrogenase activity by 2,3,7,8-tetrachlorodibenzo-*p*-dioxin. *Biochem Biophys Res Commun* **281:**1093–1099.

Takeuchi T, Katsume A, Tanaka T, Abe A, Inoue K, Tsukiyama-Kohara K, Kawaguchi R, Tanaka S, and Kohara M (1999) Real-time detection system for quantification of hepatitis C virus genome. *Gastroenterology* **116:**636–642.

Tateno C, Yoshizane Y, Saito N, Kataoka M, Utoh R, Yamasaki C, Tachibana A, Soeno Y, Asahina K, Hino H, Asahara T, Yokoi T, Furukawa T, and Yoshizato K (2004) Near completely humanized liver in mice shows human-type metabolic responses to drugs. *Am J Pathol* **165:**901–912.

Toyoda Y, Hagiya Y, Adachi T, Hoshijima K, Kuo MT, and Ishikawa T (2008) MRP class of human ATP binding cassette (ABC) transporters: historical background and new research directions. *Xenobiotica* **38:**833–862.

Umehara T, Sudoh M, Yasui F, Matsuda C, Hayashi Y, Chayama K, and Kohara M (2006) Serine palmitoyltransferase inhibitor suppresses HCV replication in a mouse model. *Biochem Biophys Res Commun* **346:**67–73.

Vee ML, Lecureur V, Stieger B, and Fardel O (2009) Regulation of drug transporter expression in human hepatocytes exposed to the proinflammatory cytokines tumor necrosis factor-$\alpha$ or interleukin-6. *Drug Metab Dispos* **37:**685–693.

Wakita T (2007) HCV research and anti-HCV drug discovery: toward the next generation. *Adv Drug Deliv Rev* **59:**1196–1199.

Wakita T (2006) Host-specific response to HCV infection in the chimeric SCID-beige/Alb-uPA mouse model: role of the innate antiviral immune response. *PLoS Pathog* **2:**e59.

Williams JA, Hyland R, Jones BC, Smith DA, Hurst S, Goosen TC, Peterkin V, Koup JR, and Ball SE (2004) Drug-drug interactions for UDP-glucuronosyltransferase substrates: a pharmacokinetic explanation for typically observed low exposure (AUCi/AUC) ratios. *Drug Metab Dispos* **32:**1201–1208.

World Health Organization (1999) Global surveillance and control of hepatitis C. Report of a WHO Consultation organized in collaboration with the Viral Hepatitis Prevention Board, Antwerp, Belgium. *J Viral Hepat* **6:**35–47.


**Address correspondence to:** Dr. Adrian J. Fretland, Hoffmann-La Roche, 340 Kingsland St., Bldg. 123/1331, Nutley, NJ 07110-1199. E-mail: adrian.fretland@roche.com

# LETTER

doi:10.1038/nature09574

# Transcriptional activation of polycomb-repressed genes by ZRF1

Holger Richly[1], Luciana Rocha-Viegas[1], Joana Domingues Ribeiro[1], Santiago Demajo[1], Gunes Gundem[2], Nuria Lopez-Bigas[2], Tekeya Nakagawa[3], Sabine Rospert[4], Takashi Ito[3] & Luciano Di Croce[1,5]

**Covalent modification of histones is fundamental in orchestrating chromatin dynamics and transcription[1–3]. One example of such an epigenetic mark is the mono-ubiquitination of histones, which mainly occurs at histone H2A and H2B[4–6]. Ubiquitination of histone H2A has been implicated in polycomb-mediated transcriptional silencing[7–9]. However, the precise role of the ubiquitin mark during silencing is still elusive. Here we show in human cell lines that ZRF1 (zuotin-related factor 1) is specifically recruited to histone H2A when it is ubiquitinated at Lys 119 by means of a novel ubiquitin-interacting domain that is located in the evolutionarily conserved zuotin domain. At the onset of differentiation, ZRF1 specifically displaces polycomb-repressive complex 1 (PRC1) from chromatin and facilitates transcriptional activation. A genome-wide mapping of ZRF1, RING1B and H2A-ubiquitin targets revealed its involvement in the regulation of a large set of polycomb target genes, emphasizing the key role ZRF1 has in cell fate decisions. We provide here a model of the molecular mechanism of switching polycomb-repressed genes to an active state.**

To identify proteins capable of binding ubiquitinated H2A (H2Aub), we developed an affinity purification based on the expression of Flag-tagged histone H2A. Among several potential H2Aub-binding proteins (Supplementary Fig. 1A, C and Supplementary Table 1), we chose to analyse ZRF1 in more depth, as within its carboxy terminus this protein contains two SANT domains, which are often found in subunits of chromatin-remodelling complexes (Fig. 1a). Intriguingly, its yeast homologue Zuo1 is linked to the ubiquitination of histone H2B in *Saccharomyces cerevisae*[10]. Moreover, ZRF1 has also been implicated in cancer and differentiation[11–13]. It adopts an oligomeric conformation and is located in the nucleus as well as in the cytosol (Supplementary Figs 1D, E and 2A). Purification of mononucleosomes from 293T cells expressing Flag-tagged histone H2A, either wild type or mutated (KKRR) at the ubiquitination sites (K118/K119), revealed ubiquitin-specific ZRF1 binding preferentially to the wild-type mononucleosomes (Fig. 1b and Supplementary Fig. 1B, F, H, I). Corroborating this finding, we observed specific binding of ubiquitinated wild-type nucleosomes to recombinant ZRF1 (Fig. 1c). Thus, these data point to the ubiquitin mark at histone H2A as a docking site for ZRF1.

ZRF1 shares homology in the zuotin domain with its yeast orthologue Zuo1 (Fig. 1a), which is synthetically lethal with Rad6, the E2 enzyme involved in the specific ubiquitination of histone H2B[10]. We reasoned that the conserved zuotin domain might contain the ubiquitin-binding motif[14]. Results from pull-down experiments with a GST–ubiquitin fusion protein and different recombinant ZRF1 truncation proteins allowed us to map the ubiquitin-binding domain (UBD) to a region C-terminal of the DnaJ domain (Fig. 1d). H2A ubiquitination as well as histone H3K27me3 are marks typically located in promoter regions of polycomb-silenced genes[15,16]. To test for ubiquitin-dependent recruitment of ZRF1 to chromatin, we established NT2 knockdown cell lines for ZRF1 or RING1B (a PRC1 subunit that is an E3 ligase; Fig. 1e). We then analysed occupancy at several promoter regions of polycomb-repressed genes, including *PER1*, *NF1C* (Fig. 1f) and the well-characterized *HOX* genes[15,16]. ZRF1 enrichment at the promoters clearly depended on the abundance of RING1B and on H2Aub levels (Fig. 1g, h and Supplementary Fig. 1G).

It has been shown that PRC1 is tethered to chromatin by the interaction of its subunit PC1 with a trimethyl mark on Lys 27 of histone H3 (H3K27me3)[8,16]. Using purified mononucleosomes containing either wild-type H2A or the H2A(KKRR) mutant, we observed that co-purification of the PRC1 subunits RING1B and BMI1 depended on the ubiquitination of histone H2A (Fig. 2a). In contrast, we did not find an alteration of the H3K27 methylation levels in nucleosomes devoid of the ubiquitin mark, indicating that stable maintenance of PRC1 at chromatin depends on the ubiquitin mark (Fig. 2a and Supplementary Fig. 2J). To understand the functional relationship between ZRF1 and PRC1, we characterized further the binding affinity of RING1B towards the ubiquitin residue by GST pull-down experiments (Supplementary Fig. 2B). Furthermore, after reconstituting RING1B-containing mononucleosome complexes, RING1B was efficiently released from nucleosomes following incubation with GST–ubiquitin (Fig. 2b and Supplementary Fig. 2C). This finding indicated that ZRF1 could compete with RING1B for binding at H2Aub. Indeed, ZRF1 overexpression led to displacement of the PRC1 subunits RING1B and BMI1 from chromatin, whereas ZRF1 knockdown led to an enhanced occupancy of RING1B at chromatin that caused an increase in H2A ubiquitination (Fig. 2c, d and Supplementary Fig. 2D–H). We next performed competition assays with the GST–ubiquitin substrate. When the His-tagged RING1B concentration was maintained, we observed that increasing the His–ZRF1 concentration led to a reduction of RING1B bound to the ubiquitin substrate, emphasizing the competition for the ubiquitin residue by both proteins (Fig. 2e). We then assembled recombinant RING1B–GST–ubiquitin complexes and performed pull-down experiments after adding either bovine serum albumin (BSA) alone (lane 1) or recombinant His–UBD and BSA (lanes 2 and 3). In concordance with the previous result, we observed RING1B replaced by the UBD of ZRF1 (Fig. 2f). Similarly, on reconstituted RING1B–mononucleosome complexes, ZRF1 efficiently displaced RING1B (Fig. 2g and Supplementary Fig. 2I). Finally, chromatin immunoprecipitation (ChIP) experiments in 293T cells overexpressing either ZRF1 or only the UBD, indicated an enrichment of ZRF1 or the UBD at promoters of the *HOX* gene cluster concomitantly with the displacement of the PRC1 subunits RING1B and BMI1 (Fig. 2h–i and Supplementary Fig. 2F). In contrast, neither a ZRF1 deletion mutant devoid of the UBD nor the yeast homologue Zuo1, which shows only a weak ubiquitin-binding capacity, were recruited to chromatin or were able to displace PRC1 (Supplementary Fig. 3A–C). It has been shown that depletion of RING1B, and thus H2A ubiquitination, leads to the loss of PRC2 from chromatin[17]. In agreement with this previous study, we found that PRC2 levels were reduced at KKRR mutant nucleosomes.

[1]Centre de Regulació Genòmica (CRG)/UPF, 08003 Barcelona, Spain. [2]Department of Experimental and Health Sciences, Universitat Pompeu Fabra, 08003 Barcelona, Spain. [3]Nagasaki University School of Medicine, Nagasaki 852-8523, Japan. [4]Institut für Biochemie und Molekularbiologie (ZBMZ), Universität Freiburg, 79104 Germany. [5]Institució Catalana de Recerca i Estudis Avançats (ICREA), Centre de Regulació Genòmica (CRG), PRBB, c/ Dr. Aiguader 88, 08003 Barcelona, Spain.

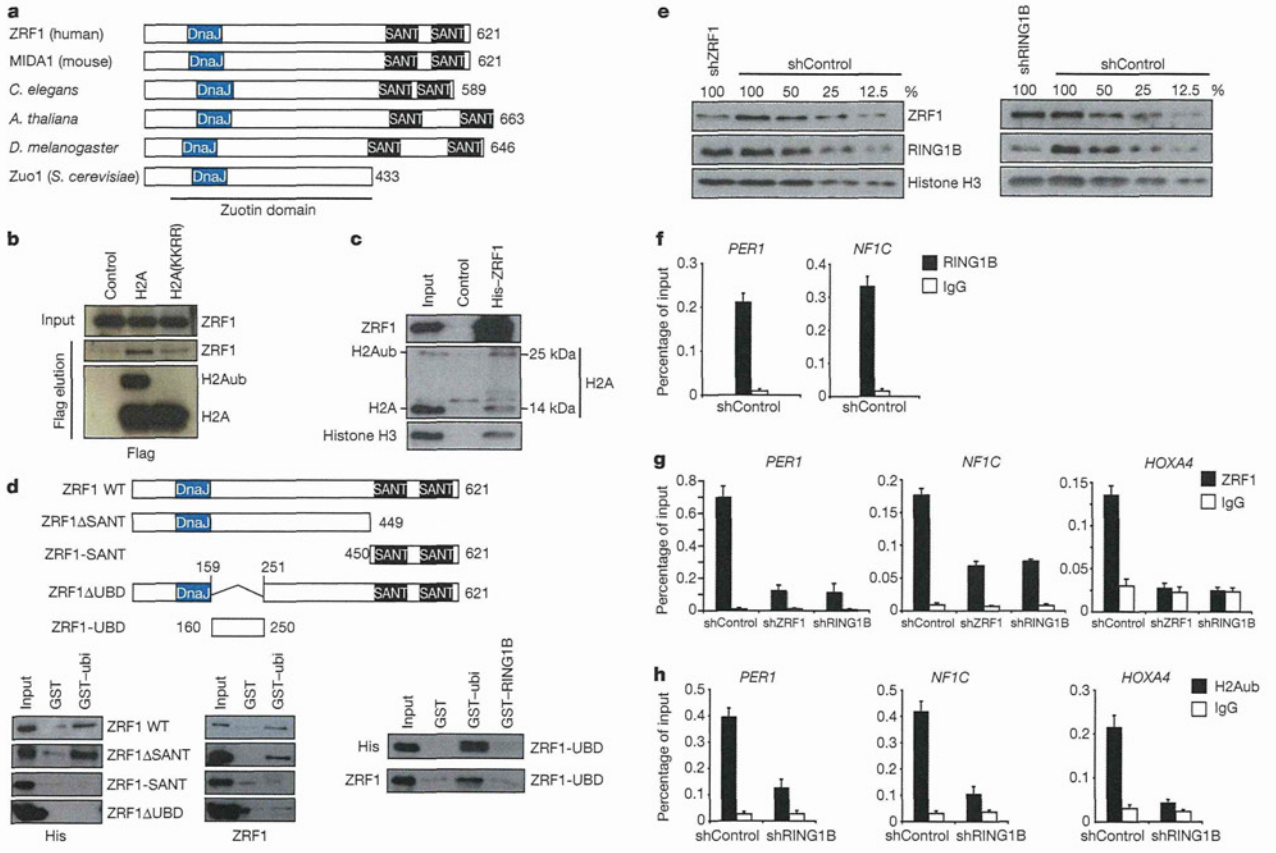


**Figure 1 | ZRF1 interacts with H2Aub.** **a**, Schematic diagram of ZRF1 orthologues indicating the DnaJ domain and SANT domains. The numbers along the right-hand side of panels **a** and **d** refer to the number of amino acids each of the proteins is composed of. **b**, Flag-tagged histone H2A and H2A(KKRR) were expressed in 293T cells. Mononucleosomes were purified and eluates were subjected to immunoblot analysis using ZRF1 and Flag antibodies. The inputs correspond to 3%. **c**, Nuclear protein extracts containing mononucleosomes were incubated with recombinant His–ZRF1. Precipitated ZRF1–nucleosome complexes were subjected to immunoblot analysis using the indicated antibodies. The inputs represent 5% of His–ZRF1 and 2% of the protein extract. **d**, GST pull-downs with GST, GST–ubiquitin (GST–ubi) and GST–RING1B (right panel) and the His-tagged proteins indicated. Bound material was subjected to immunoblot analysis using His and ZRF1 antibodies. The input shown represents 2%. WT, wild type. **e**, Protein extracts of RING1B and ZRF1 knockdown cell lines were subjected to immunoblotting and probed with the antibodies indicated in the figure. **f**, ChIP experiments performed in NT2 control cells with RING1B antibodies. **g**, **h**, ChIP experiments performed in the NT2 control and knockdown cells with ZRF1 and H2Aub antibodies. The occupancy at promoters of the *PER1*, *NF1C* and *HOXA4* genes was tested by quantitative PCR. Data are represented as mean ± s.e.m. ($n = 3$).

Similarly, PRC2 levels decreased upon binding of ZRF1 to chromatin (Supplementary Fig. 4A–C).

To globally identify ZRF1 target genes, we performed a ChIP-on-chip (see Methods) analysis in NT2 cells[18,19]. Because our data indicate that ZRF1 might antagonize silencing by polycomb proteins, we designed an experiment that allowed us to study the occupancy of ZRF1 under conditions of retinoic-acid-induced differentiation (Fig. 3a). We found ZRF1 to be enriched in 758 (not induced), 2,295 (induced for 1 h) or 995 (induced for 3 h) genes (Fig. 3b and Supplementary Table 2). Analysis of the ZRF1 occupancy at its target genes revealed a marked increase at 1 h of induction (Fig. 3b, Supplementary Fig. 5C and Supplementary Table 2). Clustering the target genes with respect to their cellular functions indicates a role for ZRF1 in developmental processes and differentiation (Fig. 3c, d and Supplementary Fig. 5A, B). Additional ChIP-on-chip analysis indicates that RING1B and H2Aub target genes are mainly involved in developmental processes (Supplementary Figs 7A–L, 8A–J and Supplementary Tables 4 and 5), as shown in previous publications[20,21]. The overlap of ZRF1 targets (1 h retinoic acid) with RING1B and H2Aub targets led to the identification of 1,102 common target genes (Fig. 3e, f). Moreover, comparison of ZRF1 target genes with polycomb target genes[22] indicates that ZRF1 is more closely linked to PRC1 than to PRC2 (Supplementary Figs 6A, B, 8K, L). We next performed a gene expression analysis comparing short hairpin RNA targeting *ZRF1* (shZRF1) with shControl (non-specific shRNA constructs) cells, with or without retinoic-acid treatment. Interestingly, downregulated genes in shZRF1 after retinoic-acid stimulation are ZRF1 or polycomb targets, particularly for PRC1 and H2Aub (Supplementary Figs 6C, 9A–G and Supplementary Table 6). Among these genes more than a hundred are targeted by ZRF1, RING1B and H2Aub and many of these are major players in developmental pathways (Fig. 4a, b). To corroborate our findings, we performed ChIP experiments and gene expression analysis on selected ZRF1 target genes. We found that ZRF1 was significantly enriched at these genes only after stimulation with retinoic acid (Fig. 4c and Supplementary Fig. 10A). Under the same conditions, we observed transcriptional activation of the same genes in wild-type NT2 cells. However, in ZRF1 knockdown cells, we detected a decrease of the messenger RNA levels (Fig. 4d and Supplementary Fig. 10B). In sum, the data presented show a clear involvement of ZRF1 in the PRC1 pathway and, most importantly, that activation of genes targeted by PRC1 and H2Aub is facilitated by ZRF1.

Several polycomb target genes become activated during differentiation, concomitantly with the disappearance of the polycomb-dependent repressive marks[15,16,23,24]. Analysis of two *HOXA* genes revealed that retinoic-acid-induced transcriptional activation depended on the presence of ZRF1. In contrast, RING1B knockdown caused a more robust

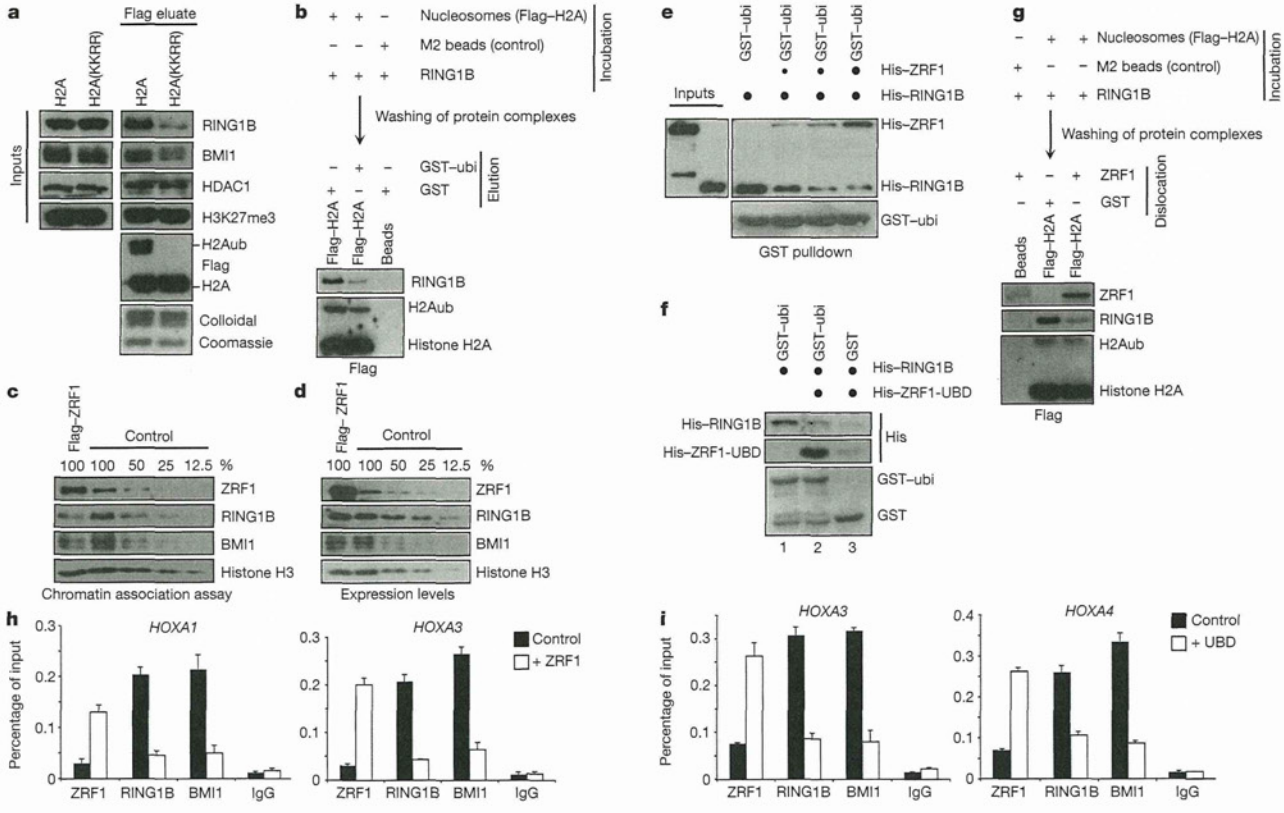


**Figure 2 | ZRF1 and PRC1 compete for binding of H2Aub.**
**a**, Mononucleosomes were purified from 293T cells expressing Flag-tagged H2A or a double mutant (KKRR). The purified material was subjected to immunoblot analysis using the indicated antibodies. The inputs represent 3%. **b**, Nucleosome–His–RING1B complexes were assembled, washed and incubated with GST (70 ng $\mu l^{-1}$) or GST–ubiquitin (70 ng $\mu l^{-1}$). Flag eluates were subjected to immunoblot analysis with the indicated antibodies. **c**, Chromatin association assay of 293T cells overexpressing ZRF1. Immunoblot analysis was performed with the indicated antibodies. **d**, Immunoblot analysis of 293T cells overexpressing ZRF1 using the indicated antibodies. **e**, GST–ubiquitin was incubated with constant amounts of His–RING1B and increasing amounts of His–ZRF1 finally reaching equimolar levels (last lane). The inputs show 10% of His–RING1B and 10% of the maximal amount of His–ZRF1. **f**, GST and GST–ubiquitin were incubated with RING1B, washed and incubated with His–ZRF1-UBD (see Methods). The retained material was subjected to immunoblot analysis with His antibodies. Lane 1 shows the pull-down in the presence of only BSA, lanes 2 and 3 in the presence of both BSA and His–ZRF1-UBD. **g**, Nucleosome–His–RING1B complexes were assembled and incubated with GST (100 ng $\mu l^{-1}$) or ZRF1 (100 ng $\mu l^{-1}$). After elution by Flag peptide, immunoblot analysis was performed with Flag, RING1B and ZRF1 antibodies. **h**, *ChIP experiments with ZRF1, RING1B and BMI1 antibodies* after overexpression of ZRF1 in 293T cells. **i**, Experiments were performed as already stated with the exception that the Flag–UBD was overexpressed instead of the full-length ZRF1. The occupancy at promoters of *HOX* genes was tested with quantitative PCR. Data are represented as mean ± s.e.m. ($n = 3$).

activation of those genes, thus supporting opposing roles for PRC1 and ZRF1 in transcriptional regulation of promoters (Fig. 4e). Next we investigated the occupancy of both ZRF1 and RING1B at promoters of *HOX* genes during retinoic-acid-induced transcription. Retinoic-acid treatment led to the recruitment of ZRF1 to promoter regions with a concomitant reduction of RING1B occupancy, clearly indicating mutually exclusive binding for these proteins at chromatin (Fig. 4f, g). Accordingly, in ZRF1 knockdown cells, RING1B was not efficiently removed from chromatin after retinoic-acid induction (Fig. 4h), as supported by previous experiments (Fig. 2a–h). In related experiments (1 h retinoic acid) we found H2Aub to be slightly reduced at *HOXA* gene promoters, indicating a deletion of this histone mark shortly after the removal of PRC1 complexes (Supplementary Fig. 11A–C). A set of similar results was obtained in retinoic-acid-induced differentiation of leukaemic cells (Supplementary Fig. 10C–E)[24]. On the basis of our results, we reasoned that ZRF1 might facilitate transcription. Recently, it has been shown that USP21-mediated H2A deubiquitination precedes gene activation[25]. To investigate further the impact of ZRF1 on transcriptional activation, we performed *in vitro* experiments testing whether ZRF1 might act in concert with specific deubiquitinases. *In vitro* deubiquitination assays carried out with mouse liver chromatin demonstrate that ZRF1 facilitates H2A deubiquitination (Fig. 4i). Thus, these results showed that, besides its function in the displacement of PRC1 complexes, ZRF1 facilitates transcription by cooperating with deubiquitinase enzymes.

Ubiquitination of H2A has long been correlated with activation of genes[26]. It is intriguing that ubiquitination of histone H2A not only has an effect on gene silencing but also is necessary to attract a factor that switches genes from a silenced to a transcriptionally activated state. However, it is still unclear how ZRF1 binding to chromatin is regulated (Supplementary Fig. 12A, B). One potential mode of regulating ZRF1, and thus cell differentiation, could be to mask its UBD domain. It has been shown that proteins of the ID (inhibitor of differentiation) family bind to ZRF1 in a region spanning its UBD domain[13] (Supplementary Fig. 12C). Our data indicate that association of PRC1 with chromatin depends on the H2Aub mark, whereas H3K27me3 is not sufficient to retain PRC1 complexes and is most probably required for its initial targeting[21,27]. RING1B/PRC1 are not as abundant as H2Aub, thus excluding a continuous binding of PRC1 complexes throughout chromatin. Yet it has been shown that during DNA damage H2A E3 ligases bind ubiquitinated H2A and propagate the initial chromatin ubiquitination marks[28]. A similar sliding mechanism could also apply to our findings regarding RING1B, and challenge the current view of ubiquitination and deubiquitination cycles (see also Supplementary

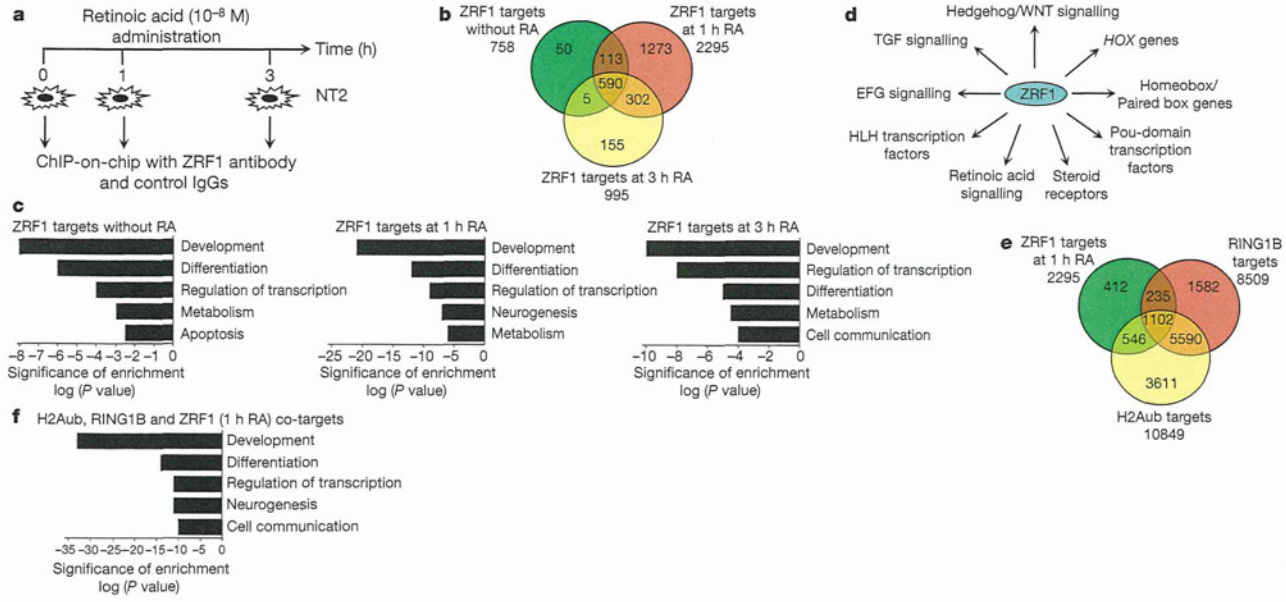


**Figure 3 | Genome-wide mapping of ZRF1 target genes in NT2 cells.** **a**, Schematic representation of the experimental approach for the ChIP-on-chip experiment. Chromatin was subjected to triplicate ChIP experiments with ZRF1 and control antibodies. The obtained material was amplified and hybridized with Human Promoter Arrays chips from Agilent. **b**, Venn diagram of the ZRF1 target genes as obtained by Chipper analysis. **c**, Functional enrichment analysis of ZRF1 target genes at the different time points of retinoic-acid (RA) induction. **d**, A selection of ZRF1 target genes identified in this study (induced for 1 h), focusing on those known to be involved in key pathways controlling cell fate decisions. **e**, Venn diagram showing significant overlapping between the gene lists of RING1B, H2Aub and ZRF1 (induced for 1 h) as obtained by ChIP-on-chip analysis. The *P* values after overlapping the H2Aub target genes with ZRF1 and/or RING1B targets are listed in the following: RING1B ($P = 10^{-16}$), ZRF1 (1 h; $P = 10^{-12}$) and RING1B-ZRF1 co-targets ($P = 10^{-16}$). **f**, Functional enrichment analysis of the 1,102 common ZRF1/RING1B/H2Aub target genes.

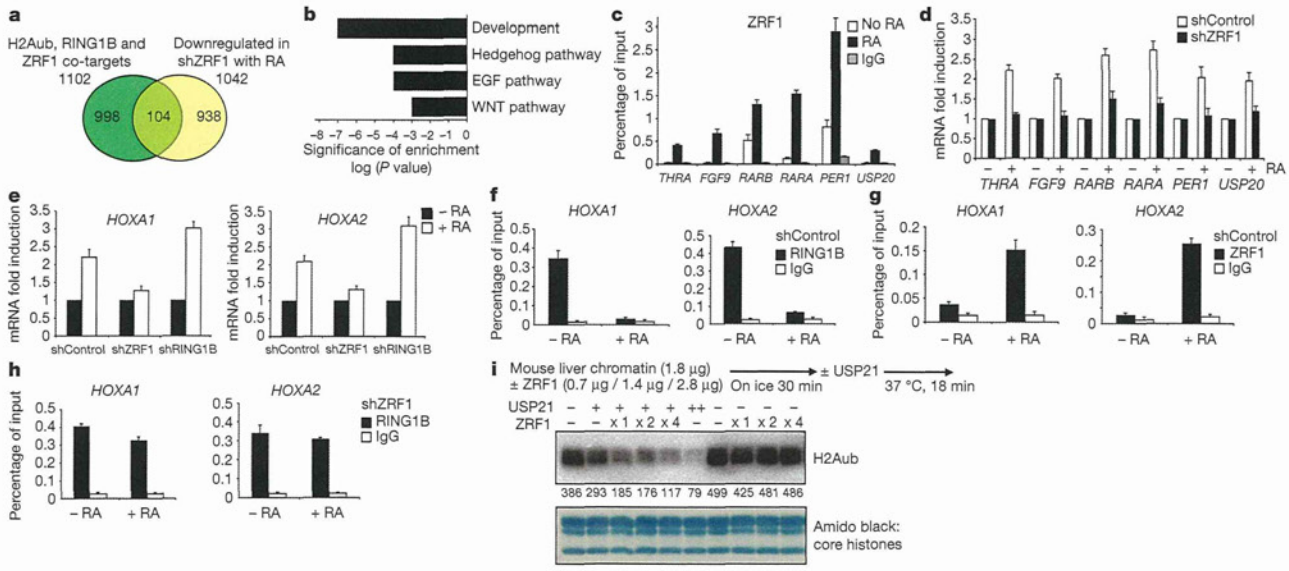


**Figure 4 | ZRF1 functions in activating polycomb-repressed genes.** **a**, The list of genes significantly repressed in comparison to shControl cells after stimulation with retinoic acid was overlapped with the common ZRF1/RING1B/H2Aub target genes (see also Supplementary Fig. 9). **b**, Functional enrichment analysis of the 104 common target genes downregulated in shZRF1 cells. **c**, ChIP experiments were performed with ZRF1 antibodies and chromatin obtained from NT2 induced with retinoic acid (*THRA*, *FGF9*, *RARB* and *RARA*: 1 h retinoic acid; *PER1* and *USP20*: 3 h retinoic acid). The occupancy at promoters of the aforementioned genes was tested by quantitative PCR. Data are represented as mean ± s.e.m. ($n = 3$). **d**, The mRNA levels of the genes indicated were measured in NT2 shZRF1 and shControl cell lines after supplementing with retinoic acid for the respective times (*THRA*, *FGF9*, *PER1* and *USP20*: 3 h retinoic acid; *RARA* and *RARB*: 2 h retinoic acid). Data are represented as mean ± s.e.m. ($n = 3$). **e**, shControl, shZRF1 and shRING1B NT2 cells were induced for 1 h with $10^{-8}$ M of retinoic acid. RNA levels of the *HOXA1* and *HOXA2* mRNA were measured in relation to mRNA levels of the ribosomal gene *PUM1* ($n = 3$). **f**–**h**, shControl NT2 cells or shZRF1 knockdown cells were kept under the same conditions as in **e**, and chromatin was used in ChIP experiments with RING1B and ZRF1 antibodies. Data are represented as mean ± s.e.m. ($n = 3$). **i**, Mouse liver chromatin was incubated with ZRF1 and USP21 (10 or 20 ng) as indicated. The H2Aub levels were quantified after detection with specific antibodies.

Discussion). However, future research will have to reveal the dynamics of PRC1-catalysed ubiquitination.

## METHODS SUMMARY

Experiments were performed using human cell lines (NT2, 293T and U937) and affinity-purified or commercially available antibodies. The knockdown cells used were established by retroviral infection. ChIP experiments, mutagenesis of histone H2A, genome-wide studies and protein purification procedures are explained in Methods.

**Full Methods** and any associated references are available in the online version of the paper at www.nature.com/nature.

**Received 12 June 2009; accepted 12 October 2010.**


1. Strahl, B. D. & Allis, C. D. The language of covalent histone modifications. *Nature* **403,** 41–45 (2000).
2. Li, B., Carey, M. & Workman, J. L. The role of chromatin during transcription. *Cell* **128,** 707–719 (2007).
3. Kouzarides, T. Chromatin modifications and their function. *Cell* **128,** 693–705 (2007).
4. Goldknopf, I. L. *et al.* Isolation and characterization of protein A24, a "histone-like" non-histone chromosomal protein. *J. Biol. Chem.* **250,** 7182–7187 (1975).
5. Zhu, B. *et al.* Monoubiquitination of human histone H2B: the factors involved and their roles in *HOX* gene regulation. *Mol. Cell* **20,** 601–611 (2005).
6. Nickel, B. E., Allis, C. D. & Davie, J. R. Ubiquitinated histone H2B is preferentially located in transcriptionally active chromatin. *Biochemistry* **28,** 958–963 (1989).
7. Wang, H. *et al.* Role of histone H2A ubiquitination in Polycomb silencing. *Nature* **431,** 873–878 (2004).
8. Kuzmichev, A., Nishioka, K., Erdjument-Bromage, H., Tempst, P. & Reinberg, D. Histone methyltransferase activity associated with a human multiprotein complex containing the Enhancer of Zeste protein. *Genes Dev.* **16,** 2893–2905 (2002).
9. Zhou, W. *et al.* Histone H2A monoubiquitination represses transcription by inhibiting RNA polymerase II transcriptional elongation. *Mol. Cell* **29,** 69–80 (2008).
10. Pan, X. *et al.* A DNA integrity network in the yeast *Saccharomyces cerevisiae*. *Cell* **124,** 1069–1081 (2006).
11. Greiner, J. *et al.* Characterization of several leukemia-associated antigens inducing humoral immune responses in acute and chronic myeloid leukemia. *Int. J. Cancer* **106,** 224–231 (2003).
12. Resto, V. A. *et al.* A putative oncogenic role for MPP11 in head and neck squamous cell cancer. *Cancer Res.* **60,** 5529–5535 (2000).
13. Inoue, T., Shoji, W. & Obinata, M. MIDA1, an Id-associating protein, has two distinct DNA binding activities that are converted by the association with Id1: a novel function of Id protein. *Biochem. Biophys. Res. Commun.* **266,** 147–151 (1999).
14. Hicke, L., Schubert, H. L. & Hill, C. P. Ubiquitin-binding domains. *Nature Rev. Mol. Cell Biol.* **6,** 610–621 (2005).
15. Bracken, A. P., Dietrich, N., Pasini, D., Hansen, K. H. & Helin, K. Genome-wide mapping of Polycomb target genes unravels their roles in cell fate transitions. *Genes Dev.* **20,** 1123–1136 (2006).
16. Lee, M. G. *et al.* Demethylation of H3K27 regulates polycomb recruitment and H2A ubiquitination. *Science* **318,** 447–450 (2007).
17. Saito, S. *et al.* Haptoglobin-β chain defined by monoclonal antibody RM2 as a novel serum marker for prostate cancer. *Int. J. Cancer* **123,** 633–640 (2008).
18. Andrews, P. W. Retinoic acid induces neuronal differentiation of a cloned human embryonal carcinoma cell line *in vitro*. *Dev. Biol.* **103,** 285–293 (1984).
19. Andrews, P. W. *et al.* Pluripotent embryonal carcinoma clones derived from the human teratocarcinoma cell line Tera-2. Differentiation *in vivo* and *in vitro*. *Lab. Invest.* **50,** 147–162 (1984).
20. Boyer, L. A. *et al.* Polycomb complexes repress developmental regulators in murine embryonic stem cells. *Nature* **441,** 349–353 (2006).
21. Kallin, E. M. *et al.* Genome-wide uH2A localization analysis highlights Bmi1-dependent deposition of the mark at repressed genes. *PLoS Genet.* **5,** e1000506 (2009).
22. O'Geen, H. *et al.* Genome-wide analysis of KAP1 binding suggests autoregulation of KRAB-ZNFs. *PLoS Genet.* **3,** e89 (2007).
23. Pasini, D., Bracken, A. P., Hansen, J. B., Capillo, M. & Helin, K. The polycomb group protein Suz12 is required for embryonic stem cell differentiation. *Mol. Cell. Biol.* **27,** 3769–3779 (2007).
24. Villa, R. *et al.* Role of the polycomb repressive complex 2 in acute promyelocytic leukemia. *Cancer Cell* **11,** 513–525 (2007).
25. Nakagawa, T. *et al.* Deubiquitylation of histone H2A activates transcriptional initiation via trans-histone cross-talk with H3K4 di- and trimethylation. *Genes Dev.* **22,** 37–49 (2008).
26. Levinger, L. & Varshavsky, A. Selective arrangement of ubiquitinated and D1 protein-containing nucleosomes within the *Drosophila* genome. *Cell* **28,** 375–385 (1982).
27. Lagarou, A. *et al.* dKDM2 couples histone H2A ubiquitylation to histone H3 demethylation during Polycomb group silencing. *Genes Dev.* **22,** 2799–2810 (2008).
28. Doil, C. *et al.* RNF168 binds and amplifies ubiquitin conjugates on damaged chromosomes to allow accumulation of repair proteins. *Cell* **136,** 435–446 (2009).


**Supplementary Information** is linked to the online version of the paper at www.nature.com/nature.

**Acknowledgements** We are indebted to S. Jentsch, S. Berger, K. Helin, J. Hasskarl, R. Shiekattar, T. Zimmermann and V. Raker for antibodies and plasmids and for discussions; and to the CRG Microarray facility and Light Microscopy Facility. This work was supported by the Spanish "Ministerio de Educación y Ciencia" (BFU2007-63059), the Association for International Cancer Research (10-0177), by the AGAUR and Consolider to L.D.C., and by FOR967 to S.R.; H.R. was supported by a FEBS fellowship; J.R. by a fellowship from Fundação para a Ciência e Tecnologia; L.R.-V. by a Juan de la Cierva Fellowship; S.D. by a PFIS fellowship.

**Author Contributions** H.R. cloned, purified proteins and performed biochemical studies. H.R., L.R.-V., J.D.R. and S.D. performed ChIP analysis. G.G. and N.L.-B. performed genome-wide analysis. T.N. and T.I. performed *in vitro* transcription and deubiquitination experiments. S.R. provided essential tools. H.R. and L.D.C. designed the experiments, supervised the project and wrote the manuscript. All authors commented on the manuscript.

**Author Information** Reprints and permissions information is available at www.nature.com/reprints. The authors declare no competing financial interests. Readers are welcome to comment on the online version of this article at www.nature.com/nature. Correspondence and requests for materials should be addressed to L.D.C. (luciano.dicroce@crg.es).

## METHODS

**Plasmids, antibodies and cell lines.** Antibodies against ZRF1 and RING1B were either previously described[29], or raised in rabbits against full-length protein and affinity purified. To that end, GST fusion proteins of both proteins were cross-linked to glutathione beads and packed into polystyrol mini-columns (Pierce). Antisera were repeatedly run over the columns, washed and finally eluted in Tris buffer pH 2.5. The affinity-purified antibody was finally set to pH 8.0. For Fig. 1d the ZRF1 serum against full-length protein was used to visualize the recombinant protein deletion mutants. In all other experiments the antibody purified with GST–ZRF1ΔSANT (a ZRF1 protein lacking the C-terminal SANT domains) was used. Antibodies against H2Aub, IgM conjugating antibody and H3K4 trimethyl were obtained from Upstate antibodies. Antibodies against histone H2A and the histone modification H3K4 trimethyl were purchased from Abcam. Antibodies against the His and Flag epitopes were purchased from Qiagen and SIGMA, respectively. Antibodies against EED and SUZ12 were a gift from K. Helin. Plasmids for the ectopic expression of Flag-tagged ID proteins were a gift from J. Hasskarl. For tagging proteins the pet28 (His tag, Novagen), pCMV2 (Flag, Invitrogen) and pGex (GST, Invitrogen) vector series were used. The ZRF1 specific sequences GTTATCTGATCCAGTGAAA and GATCAAAGCAGCTCATAAA were used to synthesize oligonucleotides and cloned into pRetroSuper[30]. In the case of RING1B the specific sequences AGAACACCATGACTACAAA and TTCTAAAGCTAACCTCACA were cloned into the same vector. Mutagenesis of histone H2A was performed using the Quikchange mutagenesis kit (Stratagene) on a pCMV2b histone H2A plasmid. Information on the cloning and sequences are available upon request. The embryonic carcinoma cell line NTERA2 (NT2/D1) and HEK 293T cells were cultured in DMEM medium supplemented with 10% fetal bovine serum at 37 °C and 5% $CO_2$. NT2 cells were treated with retinoic acid to induce differentiation at the given concentrations for the mentioned time intervals. U937 cells were cultured in RPMI medium at 37 °C and 5% $CO_2$.

**Purification of recombinant proteins.** Proteins were purified as suggested by Qiagen (His-tagged proteins) and Amersham (GST-tagged proteins) after inducing BL21 bacterial strains transformed with the respective plasmids at an optical density of 0.5 with 0.2 mM of isopropyl-β-D-thiogalactoside either for 4 h at 37 °C or at 20 °C for 14 h.

**Purification of ubiquitin-binding proteins.** HEK 293T cells were transfected with pCMV2b-histone H2A or the corresponding empty vector (Control) and after 48 h mononucleosomes were purified by means of the Flag epitope as stated in Supplementary Fig. 1A, C. After harvesting by centrifugation, cells were resuspended in buffer A (10 mM HEPES pH 7.9, 1.5 mM $MgCl_2$, 10 mM KCl and 0.5 mM dithiothreitol (DTT), phenylmethylsulphonyl fluoride (PMSF)) and homogenized by 10 strokes in a Dounce homogenizer with a B-type pestle. After centrifugation, nuclei were resuspended in lysis buffer (137 mM NaCl, 2.7 mM KCl, 10 mM $NaH_2PO_4$, 2 mM $KH_2PO_4$, 0.1% Triton X-100, 0.5 mM DTT, PMSF) and sonified using a Diagenode Bioruptor to obtain mononucleosomes (4 °C, 4 cycles of 15 min, 'H' setting). Protein extracts were then subjected to centrifugation (16,100*g*, 4 °C, 30 min) to remove debris and incubated with M2-Flag Agarose beads. The bound material or the control beads (M2-beads incubated with protein extracts from control transfections) were poured in polystyrol mini-columns (Flag–H2A column and Control column), washed intensively with lysis buffer and then used subsequently in an affinity purification. To this end, a nuclear protein extract devoid of histone proteins was prepared from 293T cells as previously described[31]. In brief, nuclei were extracted by resuspension of cells in buffer A (10 mM HEPES pH 7.9, 1.5 mM $MgCl_2$, 10 mM KCl and 0.5 mM DTT, PMSF) and homogenized by 10 strokes in a Dounce homogenizer with a B-type pestle. The crude nuclei were resuspended in buffer C (20 mM HEPES pH 7.9, 25% (v/v) glycerol, 1.5 mM $MgCl_2$, 420 mM NaCl, 0.2 mM EDTA, 0.5 mM DTT and PMSF) and homogenized in a Dounce homogenizer (10 strokes, B-type pestle). The resulting protein suspension was stirred by a magnetic stirring bar for 30 min at 4 °C and then centrifuged at 25,000*g* in an SS34 rotor for 3 h. The resulting supernatant was dialysed against lysis buffer, and run in a loop over two polystyrol mini-columns (Flag–H2A column and Control column; see above). After intensive washing with lysis buffer the columns were incubated with a solution of lysis buffer with recombinant His-tagged ubiquitin previously purified by Ni-NTA Agarose (Qiagen) and gel filtration on a Superose 12 column. After eluting the ubiquitin-binding proteins, the columns were washed again in lysis buffer and mononucleosomes were subsequently eluted by a solution of Flag peptide in lysis buffer. Both eluates were subjected to electrophoresis, stained with colloidal coomassie, and possible interactors were subjected to MALDI-Fingerprint analysis.

**Transfection and retroviral infection.** Transfection of HEK 293T cells was usually performed by the calcium phosphate co-precipitation method as described[24]. pRS-based retrovirus was produced by transfecting the GP2-293 packaging cell line (Clontech). The collected retrovirus was subsequently used to transduce NT2 or 293T cell lines by spinoculation at 900*g* for 90 min at 32 °C in the presence of protamine sulphate. After incubating overnight at 37 °C the protocol was repeated for two consecutive days.

**M2-Flag affinity chromatography.** Purification of Flag-tagged proteins from 293T cells was essentially done as described earlier. All experiments with Flag-tagged histone H2A were performed in polystyrene mini-columns (Pierce) with subsequent elution using the Flag peptide (Sigma) at a concentration of 100 μg $ml^{-1}$ in PBS.

**ZRF1–H2Aub interaction experiments.** Nuclear protein extracts were prepared as described earlier to obtain mononucleosomes. The protein extract was then incubated with or without recombinant His–ZRF1 (lanes ZRF1 and Control in Fig. 1c) for 4 h at 4 °C. Ni-NTA Agarose was added and after 2 h of incubation at 4 °C the beads were washed intensively with lysis buffer. The precipitated material was then subjected to western blotting.

**Nucleosome–RING1B complexes and *in vitro* assays.** Mononucleosomes were purified as described earlier, but washed with lysis buffer containing 450 mM NaCL and maintained at the Flag-M2 Agarose beads. The bound nucleosomes and empty M2 beads were subsequently incubated with bacterial extracts in lysis buffer containing recombinant His–RING1B. After 2 h of incubation at 4 °C the beads were washed in the same buffer intensively (see Supplementary Fig. 2C). The RING1B–nucleosome complexes were then incubated with equal or equimolar amounts of either GST or GST–ubiquitin (Fig. 2b) or ZRF1 (Fig. 2g) in lysis buffer. After 2 h of incubation at 4 °C the beads were packed into polystyrole columns, washed and eluted with Flag peptide at 100 μg $ml^{-1}$. The eluate was finally subjected to immunoblotting.

**ChIP.** ChIP experiments were essentially performed as described[24]. For all experiments affinity-purified antibodies were used as described earlier. The immunoprecipitated DNA was quantified by real-time quantitative PCR (Roche Lightcycler). The primers for verifying the occupancy of the immunoprecipitated protein at chromatin are available upon request.

**Genome-wide mapping of ZRF1 target genes (ChIP-on-chip).** Chromatin from NT2 cells before (0 h) and after induction with retinoic acid ($10^{-8}$ M) for 1 h or 3 h was subjected to ChIP experiments with ZRF1 and control antibodies. For each time-point of the ChIP experiments triplicates were carried out. The obtained material was amplified with the WGA kit (Sigma) and linear amplification of the material was tested in qPCR reactions with known ZRF1 targets. Labelling and hybridization to Agilent Human Promoter Arrays were carried out following the supplier's instructions. Analogously, chromatin from unstimulated NT2 cells was subjected to ChIP experiments with RING1B, H2Aub and the respective conjugating antibody. The obtained material was processed as described earlier.

**Microarray analysis.** Microarray analysis was performed after extracting a triplicate of three different biological samples of RNA from NT2 cells lines (shZRF1 and shControl) either from non-induced cells or cells induced with retinoic acid ($10^{-8}$ M, 3 h). RNA was amplified, labelled and subsequently hybridized to a Human Genome Oligo Microarray (Agilent). Raw data were analysed using the Limma package.

**Data analysis and statistics.** Absolute foreground and background readings from channels were used as input to the chipper program. Default parameters were used as defined previously[32]. Chipper calculates $q$ values (corrected $P$ values), thus accounting for multiple testing corrections per probe. Probes with $q$ values $<0.05$ were accepted as significant. Probes, which are significantly bound by ZRF1, were compared to those significantly bound by IgG to subtract IgG targets. ZRF1 targets were mapped to genes according to the information provided by Agilent. To study significant overlapping between genes bound by ZRF1 and genes bound by SUZ12, RING1B, H2Aub or the H3K27me3 mark, respectively, the enrichment analysis (EA) method was applied. The statistical significance ($P$ value) was calculated using the binomial distribution. Significance levels were corrected for multiple comparisons with the Benjamini and Hochbert method. Functional enrichment analysis was performed with the DAVID software[33].

**RNA preparation and analysis by quantitative PCR.** RNA was extracted with the RNeasy mini kit (Qiagen) and transcribed to cDNA by reverse transcription using the AMV kit (Roche). The expression of the respective genes was assayed by quantitative real-time PCR (Roche Lightcycler). As a reference, the expression of GAPDH or PUM1 was measured for each experiment. The sequences of the primers are available upon request.

**GST pull-down.** Purified GST–proteins were bound in equimolar amounts to glutathione beads (Amersham) in binding buffer (20 mM Tris pH 8.0, 150 mM NaCl, 0.5% NP-40). Loaded beads were washed in the same buffer and used for incubation with recombinant proteins for 2 h at 4 °C. For the competition assay (Fig. 2e) with recombinant ZRF1 and RING1B, the amounts of RING1B were kept constant and the amounts of ZRF1 were increased with every consecutive pull-down until finally reaching equimolar conditions. For preassembling RING1B–ubiquitin complexes (Fig. 2f), GST and GST–ubiquitin were bound to beads,

washed and incubated with RING1B at 4 °C for 2 h. Loaded beads were then incubated with a roughly tenfold higher amount of ZRF1-UBD together with an excess of BSA—where stated—for 90 min at 4 °C. Finally, beads were washed intensively in binding buffer, denatured in SDS buffer, and subjected to electrophoresis and subsequent western blotting analysis.

**Gel-filtration analysis.** Gel-filtration was performed on an AEKTA-Explorer system (Amersham) using Superose12 or Superose6 columns (Amersham). After calibrating the column with specific proteins, a solution of recombinant protein in PBS was injected and the UV-elution profile was detected. To verify each volume of elution the fractions were subjected to western blotting by probing with specific antibodies.

**Chromatin association assays.** Cells were crosslinked with a solution of 1% formaldehyde in PBS for 10 min at 24 °C. Nuclei were prepared by resuspending the cell pellets in buffer A (100 mM Tris pH 7.5, 5 mM $MgCl_2$, 60 mM KCl, 0.5 mM DTT, 125 mM NaCl, 300 mM sucrose, 1% NP-40). After lysis on ice the nuclei were pelleted and resuspended in buffer B (100 mM Tris pH 7.5, 1 mM $CaCl_2$, 60 mM KCl, 0.5 mM DTT, 125 mM NaCl, 300 mM sucrose) and supplemented with 10 U of MNase I for 20 min at 37 °C. The reaction was stopped by adding EDTA. The chromatin was pelleted and resuspended in buffer C (1% SDS, 10 mM EDTA, 50 mM Tris pH 8.0) overnight at 4 °C. After centrifugation (16,100*g*, 2 min) the supernatant was used for western blotting.

***In vitro* deubiquitination assays.** Deubiquitination experiments were essentially performed as previously described[25]. In short, mouse liver chromatin was incubated with no or increasing amounts of recombinant ZRF1. Subsequently USP21 was added and reactions were incubated at 37 °C for 18 min.


29. Otto, H. *et al.* The chaperones MPP11 and Hsp70L1 form the mammalian ribosome-associated complex. *Proc. Natl Acad. Sci. USA* **102,** 10064–10069 (2005).
30. Brummelkamp, T. R., Nijman, S. M., Dirac, A. M. & Bernards, R. Loss of the cylindromatosis tumour suppressor inhibits apoptosis by activating NF-κB. *Nature* **424,** 797–801 (2003).
31. Dignani, J. D., Lebovitz, R. M. & Roeder, R. G. Accurate transcription initiation by RNA polymerase II in a soluble extract from isolated mammalian nuclei. *Nucleic Acids Res.* **11,** 1475–1489 (1983).
32. Gibbons, F. D., Proft, M., Struhl, K. & Roth, F. P. Chipper: discovering transcription-factor targets from chromatin immunoprecipitation microarrays using variance stabilization. *Genome Biol.* **6,** R96 (2005).
33. Huang, D. W., Sherman, B. T. & Lempicki, R. A. Systematic and integrative analysis of large gene lists using DAVID bioinformatics resources. *Nature Protocols* **4,** 44–57 (2009).

OPEN ACCESS Freely available online PLoS GENETICS

# The Meiotic Recombination Checkpoint Suppresses NHK-1 Kinase to Prevent Reorganisation of the Oocyte Nucleus in *Drosophila*

**Oscar M. Lancaster[1¤], Manuel Breuer[1], C. Fiona Cullen[1], Takashi Ito[2], Hiroyuki Ohkura[1*]**

**1** The Wellcome Trust Centre for Cell Biology, School of Biological Sciences, University of Edinburgh, Edinburgh, United Kingdom, **2** Department of Biochemistry, Nagasaki University School of Medicine, Nagasaki, Japan

## Abstract

The meiotic recombination checkpoint is a signalling pathway that blocks meiotic progression when the repair of DNA breaks formed during recombination is delayed. In comparison to the signalling pathway itself, however, the molecular targets of the checkpoint that control meiotic progression are not well understood in metazoans. In *Drosophila*, activation of the meiotic checkpoint is known to prevent formation of the karyosome, a meiosis-specific organisation of chromosomes, but the molecular pathway by which this occurs remains to be identified. Here we show that the conserved kinase NHK-1 (*Drosophila* Vrk-1) is a crucial meiotic regulator controlled by the meiotic checkpoint. An *nhk-1* mutation, whilst resulting in karyosome defects, does so independent of meiotic checkpoint activation. Rather, we find unrepaired DNA breaks formed during recombination suppress NHK-1 activity (inferred from the phosphorylation level of one of its substrates) through the meiotic checkpoint. Additionally DNA breaks induced by X-rays in cultured cells also suppress NHK-1 kinase activity. Unrepaired DNA breaks in oocytes also delay other NHK-1 dependent nuclear events, such as synaptonemal complex disassembly and condensin loading onto chromosomes. Therefore we propose that NHK-1 is a crucial regulator of meiosis and that the meiotic checkpoint suppresses NHK-1 activity to prevent oocyte nuclear reorganisation until DNA breaks are repaired.

**Citation:** Lancaster OM, Breuer M, Cullen CF, Ito T, Ohkura H (2010) The Meiotic Recombination Checkpoint Suppresses NHK-1 Kinase to Prevent Reorganisation of the Oocyte Nucleus in *Drosophila*. PLoS Genet 6(10): e1001179. doi:10.1371/journal.pgen.1001179

**Editor:** R. Scott Hawley, Stowers Institute for Medical Research, United States of America

**Received** November 25, 2009; **Accepted** September 24, 2010; **Published** October 28, 2010



**Funding:** OML and HO received a BBSRC Special Studentship and a Wellcome Trust Senior Research Fellowship, respectively. This work is supported by The Wellcome Trust (www.wellcome.ac.uk). The funders had no role in study design, data collection and analysis, decision to publish, or preparation of the manuscript.

**Competing Interests:** The authors have declared that no competing interests exist.

* E-mail: h.ohkura@ed.ac.uk

¤ Current address: Medical Research Council Laboratory for Molecular Cell Biology, Division of Life Sciences, University College London, London, United Kingdom

## Introduction

Meiosis is a specialised form of cell division that differs from mitosis in many respects, particularly during the exchange of genetic information between homologous chromosomes in recombination. In early meiotic prophase, DNA double-strand breaks (DSBs) are introduced into meiotic chromosomes by the conserved enzyme Spo11 to initiate recombination [1–4]. An elaborate structure, the synaptonemal complex, then forms between homologous chromosomes stabilising their pairing and recombination [5]. Once recombination is complete and DSBs have been repaired, the synaptonemal complex is disassembled. As these events are meiosis-specific, molecular mechanisms of meiotic prophase progression need to be established beyond our understanding of mitotic cell cycle control.

Eukaryotes have a surveillance-signalling system, the so-called meiotic recombination checkpoint (hereafter referred to as the meiotic checkpoint), which prevents meiotic progression until DSBs generated during recombination are repaired [6–8]. Many advances have been made recently in determining the mechanisms involved in the detection of and signalling downstream from DSBs [9]. In contrast, little is known about how the checkpoint signal blocks meiotic progression, except in yeast. In yeast, the Cdc28 (Cdk1)-Cyclin complex is suppressed in various ways by the meiotic checkpoint to delay or block meiotic division [10–12].

In *Drosophila*, the meiotic checkpoint was first revealed by the study of a class of mutants collectively called *spindle* (*spn*) mutants. These *spn* mutants were originally identified based on their abnormal dorsal-ventral oocyte polarity [13–16]. They also share abnormalities in a meiosis-specific organisation of chromosomes called the karyosome [14,17,16].

The meiotic checkpoint pathway is activated in *spn* mutants by persistent DSBs caused either by defects in DNA repair during recombination [18,19] or in processing of repeat-associated siRNA that suppress germline retrotransposition [20–22]. Signalling downstream of DSBs in the meiotic checkpoint requires the successive activation of two conserved kinases, Mei-41 (an ATM/ATR homologue) and Mnk/Chk2 [17,23]. Their activation blocks both oocyte polarisation and karyosome formation. Vasa was proposed to act downstream of the meiotic checkpoint to mediate both oocyte polarisation and karyosome formation [17,23], but a more recent study suggests that Vasa acts upstream of the checkpoint through involvement in processing of repeat-associated siRNA [24]. Gurken has been shown to be a downstream effector required for oocyte polarisation which is inhibited by the meiotic checkpoint [25,16], but an effector required for karyosome formation has not been identified.

## Author Summary

Meiosis is a specialised form of cell division that produces haploid gametes from diploid cells. Failures or errors in meiosis can lead to infertility, miscarriages, or birth defects. In meiosis, chromosomes first swap genetic information during recombination and then undergo two rounds of segregation. Temporal separation of these distinct meiotic events is essential for successful meiosis. To ensure this correct temporal order, the meiotic recombination checkpoint blocks meiotic progression when recombination is not completed. Adding to our understanding of this process, we here report that the conserved *Drosophila* protein kinase NHK-1 is a crucial regulator of meiosis that is controlled by the meiotic recombination checkpoint. The meiotic recombination checkpoint suppresses the activity of NHK-1 to block transitional remodelling of meiotic chromosomes in the oocyte nucleus until recombination is completed.


The karyosome is a compact cluster of meiotic chromosomes formed within the *Drosophila* oocyte nucleus [26] and similar structures are also found in human oocytes [27]. In addition to the successful completion of recombination, recent studies by us and others have shown that nucleosomal histone kinase-1 (NHK-1) is essential for karyosome formation [28,29]. NHK-1 is a Histone 2A kinase conserved from nematodes to humans (Vrk-1 in *C. elegans*, and Vrk1-3 in mammals) [30]. We showed that NHK-1 also phosphorylates Barrier-to-Autointegration Factor (BAF) to release meiotic chromosomes from the oocyte nuclear envelope during karyosome formation [31]. However nothing is known about how NHK-1 activity itself might be controlled during meiosis.

In this report, we have investigated the functional relationship between NHK-1 and the meiotic checkpoint. We found that the meiotic checkpoint suppresses NHK-1 activity to prevent reorganisation of the oocyte nucleus, including karyosome formation, synaptonemal complex disassembly and condensin loading, until DNA breaks are repaired. Therefore, we propose that NHK-1 is a critical meiotic regulator controlled by the meiotic checkpoint.

## Results/Discussion

### The meiotic checkpoint pathway is not activated in an *nhk-1* mutant

In the wild-type oocyte nucleus, meiotic chromosomes are clustered together to form a spherical body called the karyosome [26] (Figure 1C). Female sterile *nhk-1* mutations show an abnormal morphology of the karyosome, which is less compact and often attached to the nuclear envelope [28,29,31] (Figure 1B and Figure S1). A similar karyosome abnormality is also observed in the *spn* class of mutants, which were originally identified based on their abnormal oocyte polarity [13,14,16,17] (Figure 1A and Figure S1). Most *spn* mutants contain persistent DNA double stranded breaks (DSBs) in meiotic chromosomes and activate the meiotic checkpoint pathway [18–22]. Both the karyosome and polarity defects in these *spn* mutants can be rescued by inactivation of the meiotic checkpoint [17,21,23] (Figure 1D).

A possible explanation for this similarity in the karyosome defects between *nhk-1* and *spn* mutants is that *nhk-1* mutations lead to an activation of the meiotic checkpoint pathway. To test this possibility, we assessed the activation of the meiotic checkpoint pathway in an *nhk-1* mutant by examining for the persistence of DSBs on meiotic chromosomes and the presence of oocyte/embryo polarity defects. The $nhk\text{-}1^{Z3\text{-}0437}$ mutant has been previously shown to have no delay in DSB repair or polarity defects [28]. However, as this allele contains a mis-sense mutation in a residue with unknown function in the kinase domain, the phenotype may be due to the specific nature of this allele. To exclude this possibility, we examined another female sterile allele, $nhk\text{-}1^{E24/Df}$, that expresses a reduced amount of wild-type NHK-1 protein and shows karyosome defects [29,31]. To assess oocyte polarity, we examined the dorsal appendages of eggs laid by females, whose formation depends on correct dorsal-ventral axis specification in the oocyte [32]. Dorsal appendages of eggs laid by the $nhk\text{-}1^{E24/Df}$ mutant did not show abnormalities, indicating that oocyte polarity was properly established. Furthermore, immunostaining using an antibody against the phosphorylated form of the *Drosophila* H2AX variant (γ-H2Av) which accumulates at DSB sites [33] showed no detectable DSB foci at late oogenesis stages, indicating DSBs were repaired in the $nhk\text{-}1^{E24/Df}$ mutant (Figure S2). These results indicated that, unlike *spn* mutants, the meiotic

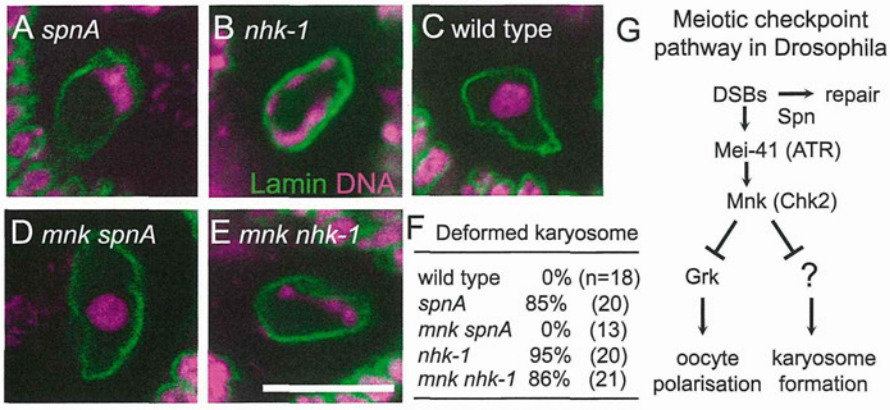


**Figure 1. Inactivation of the meiotic checkpoint did not suppress *nhk-1* karyosome defects.** The karyosome morphology in an oocyte from $spnA^{1}$ (A), $nhk\text{-}1^{E24/Df}$ (B), wild type (C), an $mnk^{p6}$ $spnA^{1}$ double mutant (D), and an $mnk^{p6}$ $nhk\text{-}1^{E24/Df}$ double mutant (E). Bar = 10 μm. (F) The frequency of deformed karyosomes in oocytes with various genotypes. Inactivation of the meiotic checkpoint by the $mnk^{p6}$ mutation rescued the karyosome defect in $spnA^{1}$ ($p<0.01$), but not in $nhk\text{-}1^{E24/Df}$ (G) The meiotic recombination checkpoint pathway in *Drosophila* oocytes (modified from 23).
doi:10.1371/journal.pgen.1001179.g001

checkpoint pathway is not activated in the *nhk-1*$^{E24/Df}$ mutant, despite the clear karyosome defect observed in this mutant.

## The karyosome defect in an *nhk-1* mutant does not require meiotic checkpoint activation

To further confirm that the karyosome defect in the *nhk-1*$^{E24/Df}$ mutant arises without meiotic checkpoint activation, we examined whether inactivating the checkpoint rescues the karyosome defect in the *nhk-1*$^{E24/Df}$ mutant. The meiotic checkpoint signalling pathway contains two kinases, Mei-41 and Mnk, which are homologues of ATM/ATR and Chk-2 respectively (Figure 1G). A mutation in either of these genes has been shown to rescue the karyosome defect caused by unrepaired DSBs in *spn* mutants (Figure 1D) [17,21,23], although *mei-41* mutations have been shown to be less proficient at rescuing the karyosome defect probably due to the presence of a second ATM/ATR homologue [21].

We constructed a double mutant between *nhk-1*$^{E24/Df}$ and *mnk* by successive genetic crosses, and immunostaining of oocytes was carried out to visualise the oocyte nucleus and the karyosome. This showed that inactivation of the meiotic checkpoint failed to rescue the karyosome defect in the *nhk-1*$^{E24/Df}$ mutant (Figure 1E and 1F). In an *mnk nhk-1* double mutant, 86% of oocytes showed deformed karyosome morphology, similar to the *nhk1* single mutant in which 95% of oocytes showed deformed karyosomes ($p>0.3$). In a control analysis done in parallel, no oocytes from an *mnk spnA* double mutant showed deformed karyosome morphology (Figure 1D and 1F), in comparison to 85% of oocytes from a *spnA* single mutant ($p<0.01$).

In conclusion, these results demonstrated that the karyosome defect in the *nhk-1*$^{E24/Df}$ mutant is not caused by activation of the meiotic checkpoint pathway.

## Unrepaired DSBs suppress NHK-1 kinase activity

The above results demonstrated that the *nhk-1*$^{E24/Df}$ mutation induces karyosome defects without activation of the meiotic checkpoint pathway. Therefore, this places NHK-1 function either downstream or in parallel to the meiotic checkpoint pathway. One way to distinguish between these two possibilities would be to examine the kinase activity of NHK-1 in oocytes under conditions activating the meiotic checkpoint pathway (ie. in *spn* mutants). It is known that NHK-1 directly phosphorylates Histone 2A (H2A) at threonine 119 (T119; 30), and this phosphorylation in the oocyte nucleus has been shown to depend on NHK-1 activity [28]. Therefore we decided to examine the level of H2A T119 phosphorylation in the oocyte nucleus as a readout of NHK-1 activity *in vivo* by immunostaining using a phospho-specific antibody (anti-dH2ApT119) [30].

Ovaries from *spn* mutants (*spnA*, *spnB*, *spnD* and *vasa*) were dissected and immunostained with the anti-dH2ApT119 antibody. As a control, we also examined wild type and the *nhk-1*$^{E24/Df}$ mutant in parallel. Compared to wild type, we found that the H2ApT119 signal was greatly reduced on meiotic chromosomes in oocytes from *spn* mutants, as well as in oocytes from the *nhk-1*$^{E24/Df}$ mutant (Figure 2A and Figure S3A).

To quantify the level of the H2ApT119 signal reproducibly and comparably between different oocytes, we measured the H2ApT119 signal in the oocyte nucleus relative to that in follicle cell nuclei, in which H2A T119 phosphorylation has been shown to be independent of NHK-1 activity [28]. H2ApT119 signals in *spn* mutants were significantly reduced ($p<0.01$; Figure 2B).

We considered the possibility that the reduction of H2ApT119 signal under meiotic checkpoint activation was simply due to abnormal karyosome morphology itself (and we were in fact measuring an artefact or a secondary consequence). First of all, this

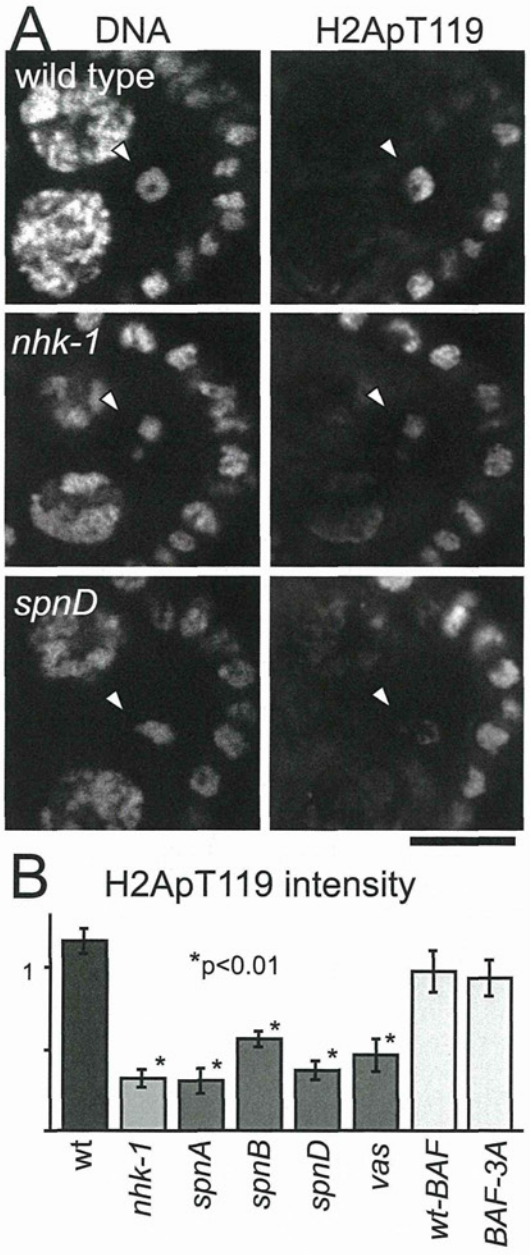


**Figure 2. Unrepaired DNA breaks suppress NHK-1 kinase activity.** (A) H2A T119 phosphorylation in wild type, *nhk-1*$^{E24/Df}$ and *spnD*$^{2}$. Ovaries at stage 5–7 were immunostained with anti-dH2ApT119 antibody and propidium iodide. Arrowheads indicate meiotic chromosomes in oocytes. Bar = 10 μm. (B) The H2ApT119 signal intensity on the chromosomes in oocytes was measured relative to that in follicle cells. The bars on the graph represent standard error of the mean (SEM). A minimum of eight oocytes from each genotype were quantified. NHK-1 activity measured by H2A T119 phosphorylation was significantly reduced in *nhk-1* and *spn* mutant oocytes ($p<0.01$; marked with asterisks). H2A T119 phosphorylation in oocytes expressing wild-type BAF and non-phosphorylatable BAF (BAF-3A) was comparable to that in wild type, indicating the karyosome abnormality itself is not the cause of low dH2ApT119 signals in *spn* mutants.
doi:10.1371/journal.pgen.1001179.g002

is unlikely because H2ApT119 signals were also reduced in karyosomes which retained relatively normal morphology in the *spn* mutants (Figure 2A and Figure S3A). To exclude this

possibility further, we took advantage of our previous study showing that expressing a non-phosphorylatable version of BAF (a substrate of NHK-1) disrupts the karyosome in these oocytes [31]. Under these conditions, although the karyosome was disrupted, the level of H2ApT119 signal in the oocyte nucleus was comparable to that in oocytes expressing wild-type BAF (that show normal karyosome morphology) or wild-type oocytes (Figure 2B and Figure S3B). Furthermore, to exclude the possibility that the apparent reduction in H2ApT119 was simply due to reduced chromosome condensation or DNA density, we re-quantified H2ApT119 signal intensity relative to DNA staining signal intensity in oocyte nuclei (Figure S3C). The H2ApT119 signal in the oocyte nucleus relative to that in follicle cell nuclei was divided by the DNA staining signal which had been measured using the same method. The result still showed a significant reduction in the H2ApT119 signal relative to DNA signal in *spn* mutant oocytes. The possibility that a simple reduction in H2A levels or its occupancy on DNA accounted for the decrease in H2Ap119 signal was further excluded by immunostaining using a phospho-independent antibody against H2A which did not show reduction in H2A signal in *spn* mutant oocytes (Figure S3D, S3E). These results confirm the genuine suppression of H2A T119 phosphorylation (which infers the suppression of NHK-1 activity) in these mutants.

Therefore we conclude that, judged by the phosphorylation level of one of its substrates, unrepaired DSBs in *spn* mutants suppress NHK-1 kinase activity in the oocyte nucleus.

## The meiotic checkpoint mediates suppression of NHK-1 activity

To confirm whether this suppression of NHK-1 activity by unrepaired DSBs is mediated by the meiotic checkpoint, we tested whether inactivation of the checkpoint (as shown in Figure 1) could abolish this suppression. Inactivation of the checkpoint was achieved by introduction of a mutation in *mnk*, which encodes the crucial checkpoint kinase Chk2. Examination of double mutants between *mnk* and *spnA* and between *mnk* and *spnD* showed that the H2ApT119 signal on meiotic chromosomes in *spn* mutants is restored by inactivation of the checkpoint (Figure 3 and Figure S4). This confirmed that the suppression of NHK-1 activity in the presence of DSBs is mediated by the meiotic checkpoint.

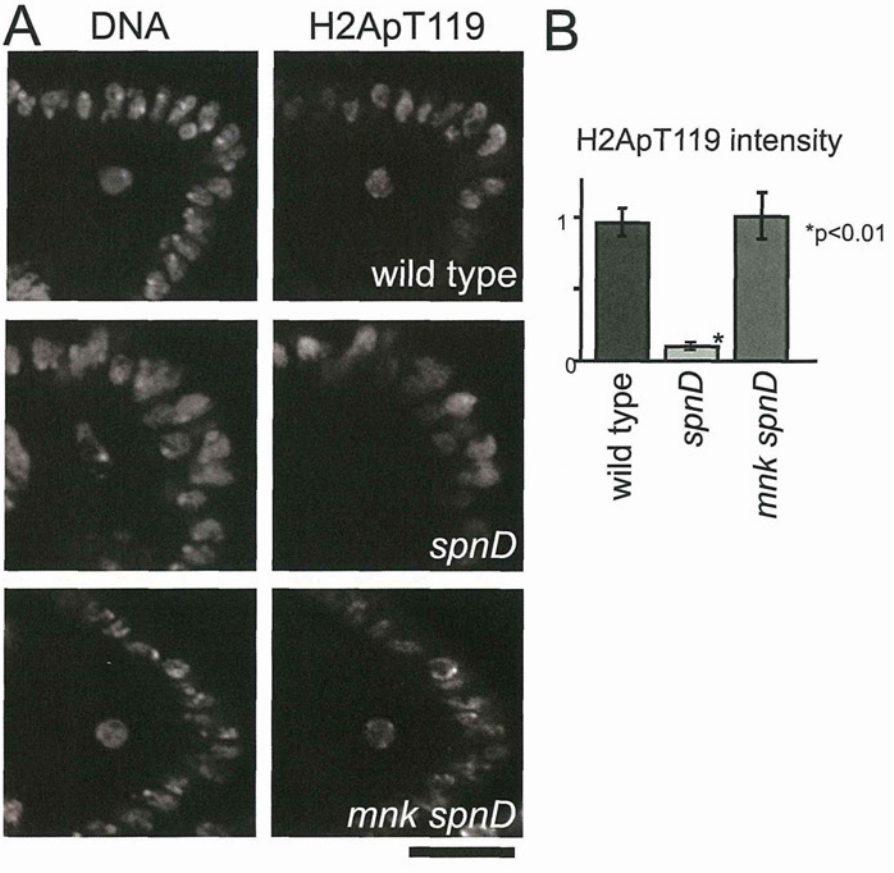


**Figure 3. The meiotic recombination checkpoint suppresses NHK-1 activity.** (A) H2A T119 phosphorylation in oocytes of wild type, *spnD*, and *mnk spnD*. Mnk (the Chk2 orthologue) is an essential kinase in the meiotic checkpoint. Ovaries at stage 5–7 were immunostained with anti-dH2ApT119 antibody and DAPI. (B) The H2ApT119 signal intensity on the chromosomes in oocytes was measured relative to that in follicle cells. The bars on the graph represent standard error of the mean (SEM). At least ten oocytes from each genotype were quantified. These samples were processed in parallel and compared only with each other, as exact values vary over time due to changes in factors including the conditions of the antibodies and fixative. NHK-1 activity measured by H2A T119 phosphorylation was significantly reduced in oocytes of a *spnD* mutant ($p<0.01$; marked with an asterisk), but not in those of an *mnk spnD* double mutant. Inactivation of the meiotic checkpoint rescued the suppression of NHK-1 activity in the presence of DSBs.
doi:10.1371/journal.pgen.1001179.g003

## DNA breaks suppress NHK-1 kinase activity in *Drosophila* cultured cells

Our cytological study showed that DSBs suppress the kinase activity of NHK-1, judged by phosphorylation of its substrate H2A at T119. We wished to confirm this suppression of NHK-1 activity by biochemical means. As biochemical measurements of oocyte-specific NHK-1 activity is challenging, we wondered whether similar suppression of NHK-1 may be observed when DSBs are induced in *Drosophila* cultured cells, without involvement of meiosis-specific factors.

To aid purification of NHK-1 from cultured cells (S2 cells), the NHK-1 gene was fused to GFP in frame and placed under the control of the metallothionein promotor. After transfection into S2 cells, a stable cell line inducibly expressing NHK-1-GFP was established. These cells were irradiated with X-rays at 1 Gy/min for 5 minutes. Immunostaining using a γ-H2Av antibody confirmed that this dose of X-rays efficiently induced DSBs without damaging the ability of cells to repair DSBs (data not shown). Fifteen minutes after X-ray irradiation, cells were collected and NHK-1-GFP was immunoprecipitated from cell extract using a GFP antibody in the presence of phosphatase inhibitors. The kinase activity of immunoprecipitated NHK-1-GFP was assayed *in vitro* by adding radioactive ATP without inclusion of exogenous substrates, as the NHK-1 substrate BAF is co-immunoprecipitated with NHK-1 [31].

Interestingly, we found that *in vitro* phosphorylation of co-immunoprecipitated BAF was greatly reduced in irradiated cells in comparison to non-irradiated cells processed in parallel (Figure 4A). This phosphorylation was dependent on NHK-1 kinase activity, as it was abolished by a mutation in NHK-1 [31] that eliminates its kinase activity but does not interfere with its binding to BAF (Figure 4A). Immunoblotting confirmed that comparable amounts of NHK-1 were immunoprecipitated from irradiated and non-irradiated samples (Figure 4A). When cells were collected 15 minutes after irradiation, their mitotic indexes were comparable (1.2% irradiated vs 1.4% non-irradiated), their nuclei still had unrepaired DSBs and nuclear localisation of NHK-1 was unaffected (Figure 4B). This indicates that the reduction in NHK-1 kinase activity in irradiated cells was not due to a reduction of mitotic cells or a change in NHK-1 localisation.

The suppression of NHK-1 kinase activity after X-ray irradiation was observed in three independent experiments. These biochemical results in S2 cells give further support to our observation in oocytes that NHK-1 kinase activity is suppressed in response to DSBs.

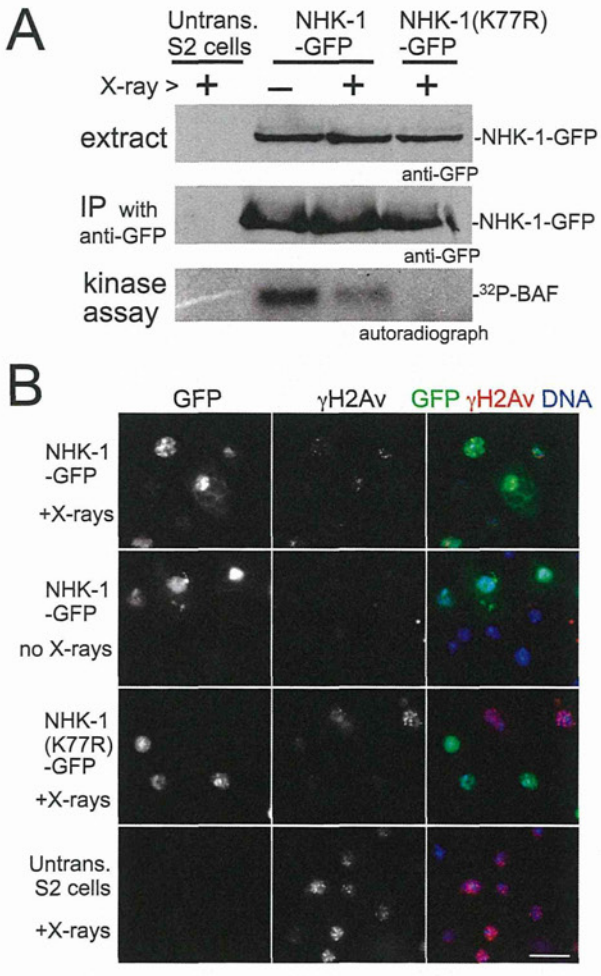


**Figure 4. DSBs suppress NHK-1 activity in S2 cells.** (A) Kinase activity of NHK-1-GFP was reduced after X-ray irradiation. S2 cells stably expressing NHK-1-GFP or NHK-1(K77R)-GFP, together with untransfected S2 cells, were irradiated with X-rays. Cells were collected 15 minutes later and NHK-1-GFP was immunoprecipitated from cell extracts by a GFP antibody. For the kinase assays, $^{32}$P-γATP was added and phosphorylation of co-immunoprecipitated BAF by NHK-1 was detected by autoradiograph. Cell extracts and immunoprecipitates used for kinase assays were immunoblotted with a GFP antibody. (B) DSBs were retained and the nuclear localisation of NHK-1-GFP was unaffected when cells were collected after X-ray treatment. DSBs and NHK-1-GFP were detected by immunostaining using antibodies against γH2Av and GFP, respectively. Bar = 10 μm.
doi:10.1371/journal.pgen.1001179.g004

## Activation of the meiotic checkpoint delays other NHK-1 dependent events

In addition to karyosome formation, NHK-1 has been shown to be required for the disassembly of the synaptonemal complex and loading of the condensin complex onto chromosomes during meiosis [28]. Our results showed that the meiotic checkpoint suppresses NHK-1 activity when DSBs are not repaired. From these observations, a prediction is that these other NHK-1 dependent events would also be blocked or delayed when the meiotic checkpoint pathway is activated. Indeed, a previous report showed that disassembly of the synaptonemal complex is delayed in a *spnA* mutant [18].

To test how universal this is, we examined the disassembly of the synaptonemal complex during oogenesis in various *spn* mutants. Immunostaining using an antibody against the synaptonemal complex protein C(3)G [34] showed that synaptonemal complex disassembly was significantly delayed in *spn* mutants. In wild-type oocytes, synaptonemal complex disassembly was completed by oogenesis stage 6. However, the characteristic filamentous structure of the synaptonemal complex or its remnants were still detected by the C(3)G antibody on meiotic chromosomes even at stage 6 or later in most oocytes of *spn* mutants (*spnA*, *spnB*, *spnD*; Figure 5A and Figure 4B). This delay in synaptonemal complex disassembly in *spn* mutants, but not in the *nhk-1*$^{c3\text{-}0437/Df}$ mutant, was reversed by inactivation of the meiotic checkpoint using an *mnk* mutation (Figure S5).

Next we examined condensin loading onto meiotic chromosomes in wild type and *spn* mutants by immunostaining. In wild-type oocytes, the conserved condensin subunit CAP-D2 [35] is fully recruited onto meiotic chromosomes by stage 6 of oogenesis. In *spn* mutants, the protein had not fully accumulated onto meiotic

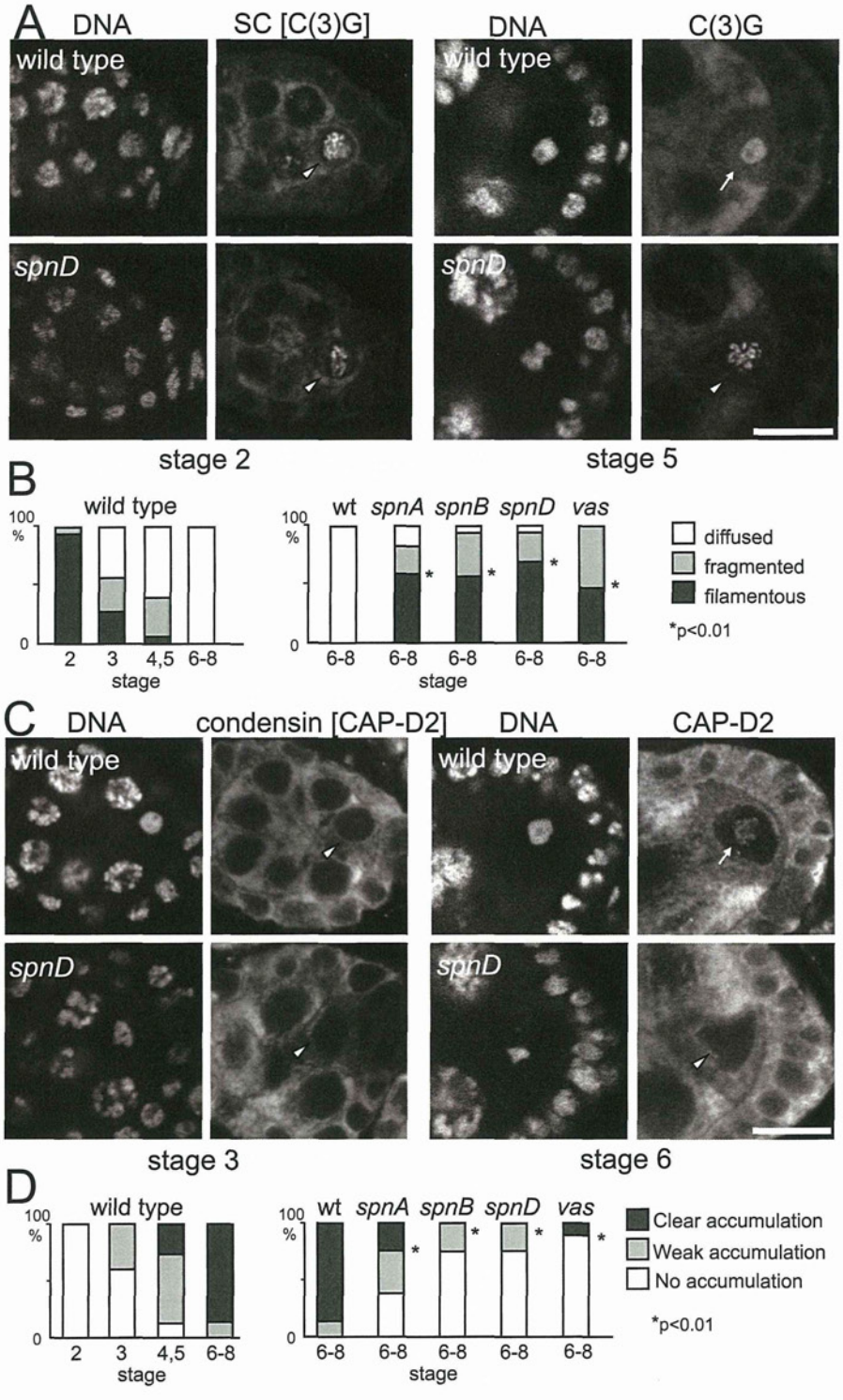


**Figure 5. Disassembly of the synaptonemal complex and loading of the condensin complex is delayed by meiotic checkpoint activation.** (A) Synaptonemal complex in wild-type and *spn* mutant oocytes. Ovaries were immunostained for the tranverse filament protein C(3)G and DNA. Bar = 10 μm. (B) The C(3)G staining pattern was classified as filamentous (arrowheads in A), fragmented or diffused (arrow in A). *spn* mutants significantly delayed disassembly of the synaptonemal complex ($p<0.01$; marked with asterisks). A minimum of thirteen oocytes were counted. (C) Condensin in wild-type and *spn* mutant oocytes. Ovaries were immunostained for the condensin subunit CAP-D2 and DNA. Bar = 10 μm. (D) Chromosome accumulation of CAP-D2 staining was classified into clear (arrow in C), weak or absent (arrowheads in C). *spn* mutants significantly delayed condensin loading ($p<0.01$; marked with asterisks). A minimum of nine oocytes were counted.
doi:10.1371/journal.pgen.1001179.g005